Investigation of the effects of viscous damping mechanisms on structural characteristics in coupled shear walls

Hadi Moghadasi Faridani [a,*], Antonio Capsoni [b]

[a] Department of Civil and Environmental Engineering, Politecnico di Milano, Leonardo da Vinci Square, 32, 20133 Milan, Italy
[b] Department of Architecture, Built Environment and Construction Engineering, Politecnico di Milano, Leonardo da Vinci Square, 32, 20133 Milan, Italy

This study addresses energy dissipation mechanisms to investigate the effects of the internal and external viscous damping on structural characteristics in coupled shear walls. A discrete *Reference Beam* (RB) is firstly proposed and a *Distributed Internal Viscous Damping* (DIVD), composed by bending and shear mechanisms, is defined. Meanwhile, the linear classical damping is considered. A low-order finite element method (FEM) is adopted for lateral analyses. For the sake of simplicity, a *Generalized Sandwich Beam* (GSB) is then developed through the replacement of the set of connecting beams of the RB by an equivalent elastic and dissipative core and a FEM is employed for its dynamic analysis. The passive damping modeling through the GSB is presented using continuous models. Concerning slender structures, the GSB is reduced to a *Coupled Two-Beam* (CTB) including the damping effects. The analytical solution of the CTB is presented to be a benchmark for the FE solutions. The validity of both numerical and analytical solutions is confirmed via numerical examples. The effectiveness of proposed damping models on dynamical responses and vibration characteristics are tested with respect to continuum-based controlling parameters, and a qualitative model is consequently proposed to appropriately choose the damping mechanisms depending upon the parameters of coupled shear walls. The suitability of various damping models is finally compared to current damping predictors and full-scale measured data given for RC buildings. The results reveal that the bending and shear damping are somehow efficient where the linear classical damping is incapable to be always a proper mechanism.

Keywords:
Tall building
Coupled shear walls
Continuum approach
Classical viscous damping
Distributed Internal Viscous Damping (DIVD)
Bending damping
Shear damping
Degree of coupling
Damping factor

1. Introduction

As commonly adopted structural systems, coupled shear walls provide a suitable solution for lateral load resisting systems in tall buildings. The overall stiffness and damping in these structures are strongly influenced not only by the mechanical and structural properties of the walls but also through the properties of the coupling elements. Since coupled shear walls are composed of multiple structural members, an equivalent continuum model [1–6] can provide a simplified tool to approximately investigate the main structural features in such structures. Apart from the stiffness properties which are extensively studied in the literature [1–4], energy dissipation mechanisms in coupled shear walls are rarely studied using continuous systems.

In order to characterize the dynamic behavior of continuous systems, vibration analysis of beams represents an important research topic in the framework of structural and mechanical engineering as it has long been studied. Indeed, given the significant influence of damping on vibration characteristics of continuous beams, wide investigations on the effects of internal, external, and distributed (continuous) dissipation sources have been con-ducted in the literature [7–12]. Due to the complex nature of these phenomena, various mathematical models of damping mechanisms have been developed so far (e.g. Newton models, fractional derivative, time hysteresis, Kelvin–Voigt and others); hence, it is important to accurately determine the relevant damping model in the analysis. From the structural engineering point of view, it has been stated [4] that the Timoshenko Beam (TB) is a suitable replacement model to analyze dynamic features of single shear walls.

Kocatürk and Şimşek [13] studied the dynamic response of eccentrically prestressed viscoelastic TBs under a moving harmonic load, characterized by a Kelvin–Voigt damping model. The results indicated that the eccentricity of the compressive load, the shear deformation, the excitation frequency of the moving harmonic load and the internal damping significantly affect the

* Corresponding author. Tel.: +39 3888190949.
E-mail addresses: hadi.moghadasi@polimi.it (H. Moghadasi Faridani), antonio.capsoni@polimi.it (A. Capsoni).

Published Journal Article available at: http://dx.doi.org/10.1016/j.engstruct.2016.02.031

Nomenclature

DIVD	Distributed Internal Viscous Damping
TB	Timoshenko Beam
EBB	Euler–Bernoulli Beam in CTB
RCB	Rotational Constrained Beam in CTB
IDTF	Inter-story Drift Transfer Function
$\mathcal{L}$	Lagrangian
$\mathcal{R}$	Rayleigh dissipation function
T	kinetic energy
$\mathcal{V}$	potential energy
c	classical viscous damping
c_{b1}, c_{b2}	internal bending dampings in left and right walls
c_{s1}, c_{s2}	internal shear dampings in left and right walls
c_ϑ, k_ϑ	equivalent rotational damping and stiffness in CTB
A_c, I_c	continuum core area and moment of inertia in GSB
ρ_d, ρ_c	walls and core masses per unit volume in GSB
W_f	work produced by external load
$f(x,t)$	distributed transverse load
A_1, A_2	cross-section areas of two walls
I_1, I_2	moments of inertia of two walls
I_{bi}, A_{bi}	moment of inertia and area of connecting beams
E, G	Young's and shear elastic modulus
ω_j, ϕ_j	complex eigenvalues and eigenvectors associated to jth mode
γ_j	complex eigenvalue parameter associated to jth mode
$\omega_{d,1}, \omega_{N,1}$	damped and natural frequency of first mode
ζ_j	modal damping ratio of jth mode
$Real(\omega_1)$, $Im(\omega_1)$	decay rate and oscillating part of first mode
K_b	sum of flexural stiffnesses of walls
$\bar{\alpha}_0^2$	controlling parameter with GSB
α_0^2	degree of coupling
ζ	damping factor associated to first mode
RB	Reference Beam
GSB	Generalized Sandwich Beam
CTB	Coupled Two-Beam
DMF	dynamic magnification factor
QEP	quadratic eigenvalues problem
κ	shear correction factor
v, φ	lateral displacement and rotation in connecting beams
h_b, ℓ_b	depth and length of connecting beams
h	story height
c_{bi}, c_{si}	bending and shear damping in ith element
η_{bi}, η_{si}	bending and shear damping multipliers in ith element
c_{b3}, c_{s3}	internal bending and shear damping in connecting beams
c_{eq}, k_{eq}	equivalent distributed shear damping and shear stiffness in GSB
c_d, k_d	viscous damping and stiffness coefficient in dampers
$c_{eq,b}$, $c_{eq,s}$	equivalent shear damping to bending and shear damping in connecting beams
$\rho(x,t)$	rotation in the core of GSB
u, $\dot{u}$, $\ddot{u}$	transverse displacement, velocity and acceleration
θ, ψ	rotations in left and right walls
μ	dimensionless coordinate in FE
$s_e(x,t)$	generalized displacement vector
$N(x)$	shape functions matrix containing linear function interpolations
B_1, B_2	widths of left and right walls
M_e, C_e, K_e	mass, damping and stiffness matrices of eth FE
M, C, K	global mass, damping and stiffness matrices
Q_e	generalized forces vector of eth FE
E_{eq}, G_{eq}	elastic moduli of equivalent core in GSB
K_{s1}	sum of shear stiffnesses of walls
K_{s2}	equivalent shear stiffness of core
IDR	inter-story drift ratio
M, V	bending moment and shear force

dynamic response of the beam. There is proposed a wide dissertation on the damped natural frequencies of a cantilever beam with Kelvin–Voigt damping and a piezo-patch actuator and sensor bonded onto it, evaluating the effect induced by their locations on the damped fundamental frequencies of the system [14].

Also more recently, the effect of the location of damped segments on the vibrations of beams with partially Distributed Internal Viscous Damping (DIVD) was investigated [15]. The vibration equations of a TB with DIVD subjected to transverse loading were derived and the transfer matrix method (TMM) was used to determine the frequency equations and to study the vibration characteristics. To demonstrate feature of DIVD effects, various damping and restraining conditions have been taken into account. The influence of the damping, length and location of damped segments on the vibration of beams with DIVD has been investigated and discussed. Some researchers [16–18] extended this latter research considering the local distribution of DIVD through the TB formulation. The effects of the damping amount, length, and location of the damped segment on the damped natural frequency of beams have been investigated and discussed. Moreover, the investigation of TBs with DIVD has been generalized referring to a shear slender-ness parameter [17].

Albeit, the TB including distributed damping models may be relevant to analyze the damped structural characteristics in single shear walls, a different behavior may be resulted in coupled shear walls, since the walls are coupled by ordinary connecting beams [1,3] or passive coupling devices [19,20].

Lavan [19] proposed a shear-type damping to model viscously coupling elements in wall systems. His continuum-based solution was including a single (shear) mechanism for both inherent and additional damping and a single (flexural) stiffness without any coupling effect (shear stiffness) due to the presence of ordinary connecting beams. A distributed classical damping was considered in the Coupled Two-Beam (CTB) [21] to model the inherent damping and the modal analysis was proposed to compute the dynamic responses of building structures.

Given the suitability of non-classical DIVD models for single (uncoupled) beam elements, this paper is devoted to further develop the concept of such damping models in coupled shear walls by employing multi-beam (continuous) systems and to shed some lights on the effects of various energy dissipation mechanisms on structural and vibrational characteristics in such coupled systems. In this study, in addition to the classical damping, the DIVD composed by bending and shear damping mechanisms are properly developed using three beam systems: Reference Beam (RB), Generalized Sandwich Beam (GSB), and Coupled Two-Beam (CTB).

The RB, which is considered as the discrete model of coupled shear walls, consists of vertical and horizontal TB elements, all including DIVD mechanisms. The GSB is then developed on the basis of the RB by replacing the set of horizontal beams with an equivalent dissipative core. Some useful GSB systems with equivalent stiffness and damping coefficients are illustrated in order to show how passive dissipating devices (e.g. viscous and viscoelastic dampers) can be equivalently modeled through continuous (smeared) effects. Dealing with tall systems, the CTB model with various DIVD effects is proposed comprising an Euler–Bernoulli Beam (EBB) and a Rotational Constrained Beam

(RCB). The numerical solutions using low order FE models are developed for the forced analysis and complex eigenanalysis of the RB and GSB and the closed-form solutions are proposed for the CTB system as a benchmark to the FEM-based results.

The effectiveness of proposed damping models on fundamental eigenproperties and structural responses is evaluated using the proposed beam models and their eligibility is analyzed with respect to appropriate controlling parameters (degree of coupling and damping factor), thus, a qualitative model is developed to choose the suitable damping mechanism. Furthermore, employing some damping predictors and measurements for buildings, the efficiency of DIVD models is tested against the classical damping. The numerical results showed the usefulness of the DIVD mechanisms to deal with both internal and external energy dissipation phenomena in coupled shear walls with different degrees of coupling and revealed some shortcomings of the linear classical damping.

2. Material and methods

In this section, three beam systems are proposed to conceptually introduce viscous (distributed) damping mechanisms in coupled shear walls, with the aim of analyzing the main structural characteristics. It should be noted that the study is devoted to those structures in which the connecting beams are weak compared to the shear walls; hence, they are incapable to transfer high enough shear forces to compress the walls or to bend them locally; thus, the global bending and local shearing are neglected. The other applications of continuum-based models which provide simple formulas for the preliminary design and immediate check of computer-based results are not in the scopes of the present study.

2.1. The Reference Beam (RB)

In this section, a cantilevered RB consisting of two main Timoshenko Beams (TB) connected by a certain number of connecting TBs is considered (Fig. 1). The RB may be presented in two fashions: undamped and damped systems. The undamped sys-tem contains all the stiffness properties and statically kinematical fields in structural elements. Then, the RB model can be equipped (damped RB) by introducing the multi-damping characteristics to the undamped system. The RB is assumed to be subjected to a homogeneously, sinusoidal in time, distributed transverse load $f(x,t)$ (see Fig. 1).

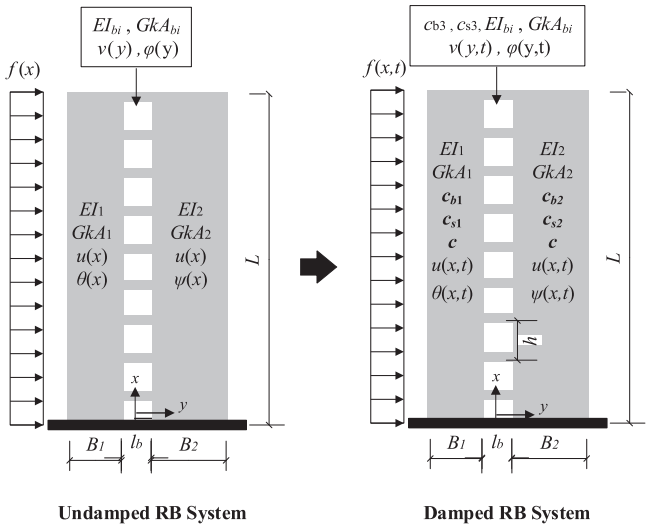

Fig. 1. Reference Beam (RB) in two fashions: Undamped system and damped system.

The transverse equations of motion of such a system are readily obtained by applying Hamilton's Principle to the Lagrangian $\mathcal{L}$ and the Rayleigh dissipation function $\mathcal{R}$ of the system obtained by assuming the kinematic model and the constitutive law of the classical Timoshenko's theory:

$$\delta \int_{t_0}^{t_1} (\mathcal{L} - \mathcal{R}) dt = \delta \int_{t_0}^{t_1} (T - \mathcal{V} + W_f - \mathcal{R}) dt = 0 \tag{1}$$

where Total Kinetic Energy T, the Potential Energy $\mathcal{V}$, and the Work W_f produced by the external transversal load are respectively expressed as:

$$T = \frac{1}{2}\rho_d \int_0^L [A_1(\dot{u})^2 + I_1(\dot{\theta})^2 + A_2(\dot{u})^2 + I_2(\dot{\psi})^2] dx \tag{2}$$

$$\mathcal{V} = \frac{1}{2}\int_0^L [EI_1(\theta')^2 + G\kappa A_1(u' - \theta)^2 + EI_2(\psi')^2 + G\kappa A_2(u' - \psi)^2] dx + \frac{1}{2}\sum_{i=1}^{n}\left[\int_0^{\ell_b} EI_{bi}(\varphi_i')^2 + G\kappa A_{bi}(v_i' - \varphi_i)^2 dy\right] \tag{3}$$

$$W_f = \int_0^L f(x,t) u dx \tag{4}$$

Note that the Kinetic Energy governed by connecting beams is neglected.

The damping model, Distributed Internal Viscous Damping (DIVD), herein assumed is such to introduce retarding and dissipative forces arising from damping effects during the motion. The DIVD is originated from the Kelvin–Voigt strain velocity damping, where bending and shear dissipative additional stresses, σ_x^d and τ_{xy}^d, linearly proportional to the strain velocity through internal damping coefficients, have to be introduced leading to the following stress–strain relations for main beams (shear walls) and also connecting beams:

$$\begin{cases} (\sigma_x)_i = (\sigma_x^e)_i + (\sigma_x^d)_i = (E\varepsilon_x)_i + c_{bi}(\dot{\varepsilon}_x)_i \\ (\tau_{xy})_i = \left(\tau_{xy}^e\right)_i + \left(\tau_{xy}^d\right)_i = (G\gamma_{xy})_i + c_{si}(\dot{\gamma}_{xy})_i \end{cases}; \quad i = \text{Number of Structural Element} \tag{5}$$

where c_{bi} and c_{si} are independently defined in main beams and connecting beams (see the damping system in Fig. 1). A further contribution is represented by the classical dissipative force directly proportional to the transverse velocity $\dot{u}(x,t)$ of the beam, through the classically linear viscous damping coefficient c. Therefore, assigning $c_{b1,2}$ and $c_{s1,2}$ to the left and right main beams and c_{b3}, c_{s3} to the set of identical connecting beams, the Rayleigh Dissipation Function can be obtained assuming the subsequent expression:

$$\mathcal{R} = \frac{1}{2}\int_0^L \left\{c_{b1}I_1\dot{\theta}'^2 + c_{s1}\kappa A_1(\dot{u}' - \dot{\theta})^2 + c_{b2}I_2\dot{\psi}'^2 + c_{s2}\kappa A_2(\dot{u}' - \dot{\psi})^2 + c\dot{u}^2\right\} dx + \frac{1}{2}\sum_{i=1}^{n}\left[\int_0^{\ell_b}\left[c_{b3}I_{bi}(\dot{\varphi}_i')^2 + c_{s3}\kappa A_{bi}(\dot{v}_i' - \dot{\varphi}_i)^2\right] dy\right] \tag{6}$$

It is worth noticing that the relationship between the internal viscous damping coefficients, c_{bi} and c_{si}, can be assumed analogously to that between Young's elastic modulus and shear elastic modulus for an isotropic material. Thus, in view of the stress–strain relations of Eq. (5), the bending and shear damping coefficients are assumed to be proportional to Young and Shear elastic modules by two independent amplification factors in main beams and connecting beams, as Eq. (7) shows [15–18]:

$$c_{bi} = \eta_{bi}E_i; \quad c_{si} = \eta_{si}G_i; \quad i = \text{Number of Structural Element} \tag{7}$$

Substituting all the relevant terms (Eqs. (2)–(4), and Eq. (6)) in Hamilton's Principle (Eq. (1)), PDEs of motion of the RB system can be straightforwardly obtained.

2.1.1. A six degrees of freedom FE system

In order to evaluate the dynamic response of the RB, the classical FEM approach is established to reduce the PDEs of motion into linear second-order ordinary differential equations with time as the independent variable. A simple low order beam FE model is therefore introduced with linear variation in displacement $u(x)$ and rotations $\theta(x)$, $\psi(x)$ resulting in six degrees of freedom (DOFs) (Fig. 2).

Dimensionless coordinate μ and nodal displacements vector of the eth generic FE are:

$$\mu = \frac{2x}{\ell}; \quad U_e = [u_1, \theta_1, \psi_1, u_2, \theta_2, \psi_2]^T \tag{8}$$

The generalized displacement vector $s_e(x,t)$ of the eth FE can be expressed as:

$$s_e(x,t) = [\,u \quad \theta \quad \psi\,]^T = N(x)U_e(t) \tag{9}$$

To accurately take the connecting beams' effects into consideration, the length of each FE is assumed equal to the story height. The displacement $v(y)$ and rotation $\varphi(y)$ in connecting beams can be defined as functions of rotations $\theta(x)$ and $\psi(x)$ in the main beams (see Appendix A) because of their connectivity in junctions. Hence, assuming that the rotations in the two ends of the connect-ing beams are identical to the rotations in the main beams, they can be expressed as follows:

$$v\left(y = -\frac{\ell_b}{2}\right) = -\frac{B_1}{2}\theta; \quad \varphi\left(y = -\frac{\ell_b}{2}\right) = \theta;$$
$$v\left(y = \frac{\ell_b}{2}\right) = \frac{B_2}{2}\psi; \quad \varphi\left(y = \frac{\ell_b}{2}\right) = \psi \tag{10}$$

Applying Lagrange's equation to any DOF ($i = 1, \ldots, 6$) of the FE, the resulting system of equations of motion assumes the subsequent expression:

$$M_e\ddot{U}_e + C_e\dot{U}_e + K_eU_e = Q_e \tag{11}$$

Considering the expressions of the Kinematic and Potential Energies (Eqs. (2) and (3)), of the Work due to the external forces (Eq. (4)), and of the Rayleigh Function (Eq. (6)), the FE matrices can be readily determined (see Appendix A).

It should be remarked that the damping contributions of the connecting beams (see C_1, C_2, and C_3 in Appendix A) are obtained using the second term of the Rayleigh Function (Eq. (6)).

By simply assembling and imposing the appropriate boundary conditions, the global system of equations of motion of the clamped RB is thus determined, assuming the classical form:

$$M\ddot{U} + C\dot{U} + KU = Q \tag{12}$$

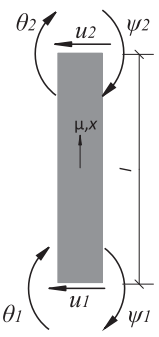

Fig. 2. One dimensional FE model with six DOFs.

In order to allow simple assemblage of the matrices and to solve the dynamic system of equations of motion, a FEM-based code is implemented in Matlab® [22]. Newmark's step-by-step method of direct integration over discrete time steps [23] is preferred to other algorithms (e.g. non-classical modal analysis which would have provided complex conjugate pairs of eigenvalues and eigenvectors) due to its higher flexibility in dealing with the different damping and loading situations of the (non-classical) problem at hand.

2.1.2. Damped eigenfrequency analysis

The system of equations of motion of the damped freely vibrating beam system assumes the following form:

$$M\ddot{U} + C\dot{U} + KU = 0 \tag{13}$$

Accordingly, introducing $U = \varphi e^{\omega t}$ into Eq. (13) yields the QEP as follows:

$$[\omega^2 M + \omega C + K]\phi = 0 \tag{14}$$

The solution of Eq. (14) provides the complex eigenvalues ω_i of the QEP and the associated eigenvectors $\emptyset$, which occur in $2n$ complex conjugate pairs for a non-classical n-DOFs system, such as the RB under analysis. The QEP requires to identify complex eigenvalues ω_i and associated non-zero eigenvectors φ_i ($i = 1, \ldots, 2n$), satisfying the subsequent associated characteristic equation:

$$\det|\omega^2 M + \omega C + K| = 0 \tag{15}$$

Considering the first complex eigenvalue ω_1, which is associated to the first mode of vibration, by adopting a notation common to the one used for a viscous-damped SDOF system [24], the *Real* and *Imaginary* parts of ω_1 can be identified by the subsequent relation:

$$\omega_1 = Real(\omega_1) + i \cdot Im(\omega_1) = -\omega_{N,1}\zeta_1 + i\omega_{N,1}\left(\sqrt{1-\zeta_1^2}\right)$$
$$= -\omega_{N,1}\zeta_1 + i\omega_{d,1} \tag{16}$$

Here, $\omega_{N,1}$ and ζ_1 can be expressed as:

$$\omega_{N,1} = \sqrt{Real^2(\omega_1) + Im^2(\omega_1)}; \quad \zeta_1 = -\frac{Real(\omega_1)}{\omega_{N,1}} \tag{17}$$

The complex eigenproperties associated to higher modes can be similarly extracted using Eq. (15).

2.2. The Generalized Sandwich Beam (GSB)

In order to analyze coupled shear walls, an equivalent rod theory [25] was developed to replace the original structure by a continuum model of one-dimensional or two-dimensional rods with equivalent stiffness and mass distributions. For the sake of simplicity in this study, the discrete set of connecting beams in the RB is replaced by an equivalent homogeneous core characterized by E_{eq} and G_{eq} (see the undamped system in Fig. 3a). The achieved continuum model, called undamped GSB, can be developed under the following assumptions:

- The wall system is in plane stress condition.
- Shear walls have rigid cross sections and connecting beams are inextensible.

As suggested [26,27], the elastic curtain equivalent to connecting beams is obtained by equating the stress energy of a typical connecting beam to the one of its equivalent continuum. The equivalent elastic modulus E_{eq} of the core is assumed equal to zero in order to assure the normal stress along the x axis to vanish.

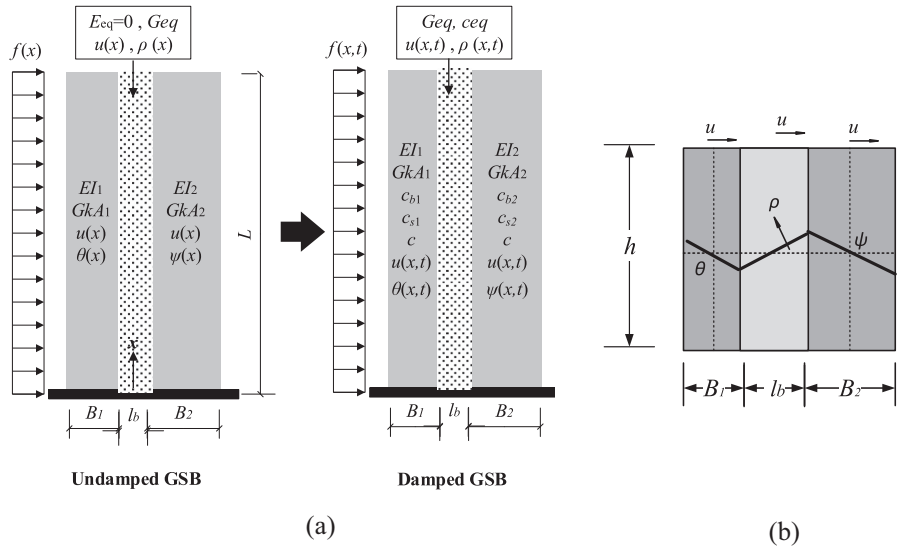

Fig. 3. (a) Generalized Sandwich Beam (GSB) as undamped and damped systems and (b) rotation fields in walls and core.

The equivalent shear modulus G_{eq} reads

$$G_{eq} = \frac{1}{ht}\left(\frac{\ell_b'^2}{12EI_b} + \frac{1}{G\kappa A_b}\right)^{-1} \tag{18}$$

Local deformation effects at junctions between the connecting beams and main beams are also taken into account in evaluating the G_{eq} through the following approximate relation

$$\ell_b' \cong \ell_b\left(1 + \varepsilon\frac{h_b}{\ell_b}\right) \tag{19}$$

Here, coefficient ε may be defined as $0 < \varepsilon \leqslant 1$, e.g. ε = 0.5 [28]. Compatibility between the rotations in the main beams and in the continuum core (see Fig. 3b) at the centroid of the beams can be expressed as the linear relationship

$$\rho(x,t) = -\frac{B_1\theta(x,t) + B_2\psi(x,t)}{2\ell_b} \tag{20}$$

Although a first-order shear deformation theory is considered in the present GSB, because of the similarity of the GSB's structure to composite systems, it may be useful to potentially investigate several advanced higher-order shear deformation theories adopted for functional graded plates [29–37]. Using these theories, there is no need to the shear correction factor in the formulation. Since the walls and core properties are different in the GSB, developing an efficient (hyperbolic) shear deformation beam theory [38] on the basis of the neutral surface position, may accurately yet simply provide the bending and free vibration analysis. To account for the normal stress in the core, in addition to the shear stress, a (refined trigonometric) higher-order theory may be proposed [39] by including the thickness stretching effect (non-zero normal strain). Employing a new modified couple stress theory [40], in which the transverse displacement may consist of the bending component in addition to the shear one, dynamic responses can be analyzed having a variable length scale parameter to capture also the size effect in the GSB.

Nevertheless, using the first-order shear deformation theory, the Potential Energy in the GSB is

$$\begin{aligned}\mathcal{V}(u,\theta,\psi) = \frac{1}{2}\int_0^L &[EI_1(\theta')^2 + G\kappa A_1(u'-\theta)^2 + EI_2(\psi')^2 \\ &+ G\kappa A_2(u'-\psi)^2 + G_{eq}(t\kappa\ell_b)(u'-\rho)^2]dx\end{aligned} \tag{21}$$

The Kinetic Energy reads

$$\begin{aligned}T(\dot{u},\dot{\theta},\dot{\psi}) = &\frac{1}{2}\int_0^L \rho_d[(A_1+A_2)\dot{u}^2 + I_1\dot{\theta}^2 + I_2\dot{\psi}^2]dx \\ &+ \frac{1}{2}\int_0^L \rho_c(A_c\dot{u}^2 + I_c\dot{\rho}^2)dx\end{aligned} \tag{22}$$

where ρ_c assumes [26]:

$$\rho_c = \frac{h_b}{h}\rho_d \tag{23}$$

The present continuum model, the undamped GSB (Fig. 3a), is then generalized by accounting for various damping models. The classical damping and DIVD mechanisms are taken into consideration; moreover, an equivalent distributed damping c_{eq} is proposed for the continuum core (see the damped GSB system in Fig. 3a). The coefficient c_{eq} can be obtained by a Rayleigh function balance between a typical connecting beam including c_{b3} and c_{s3} and its inter-story equivalent continuum. The resulting expressions associated to the bending and shear damping are then expressed, respectively:

$$c_{eq,b} = \frac{4c_{b3}I_b(m_1+m_2)^2\ell_b^2}{th(B_1+B_2)^2}; \quad c_{eq,s} = \frac{4c_{s3}A_b(m_3+m_4)^2\ell_b^2}{th(B_1+B_2)^2} \tag{24}$$

where m_1, m_2, m_3, and m_4 are listed in Appendix A.

The complete Rayleigh function in the damped GSB system is then given by:

$$\begin{aligned}\mathcal{R}(\dot{u},\dot{\theta},\dot{\psi}) = \frac{1}{2}\int_0^L &[c_{s1}\kappa A_1(\dot{u}'-\dot{\theta})^2 + c_{b1}I_1(\dot{\theta}')^2 \\ &+ c_{s2}\kappa A_2(\dot{u}'-\dot{\psi})^2 + c_{b2}I_2(\dot{\psi}')^2 \\ &+ c_{eq}(t\kappa\ell_b)(\dot{u}'-\dot{\rho})^2]dx\end{aligned} \tag{25}$$

Here, $\dot{\rho}$ is the time derivative of ρ expressed in Eq. (20). The same shape functions adopted for the RB model are chosen to be used in Eqs. (21), (22), and (25). It should be mentioned that FE structural matrices corresponding to the main beams are exactly those adopted for the RB, but the FE matrices associated to the continuum core (M_{core}, C_{core}, and K_{core}) are differently determined (see Appendix B). These latter matrices must be assembled on those of the main beams. The free and forced vibration analysis can be afforded similarly to the procedures explained in Section 2.1.

In order to define a relevant controlling parameter, a simplification is considered. It has been numerically demonstrated [41] that

the rotational fields in the walls may be almost identical ($\theta \cong \psi$), provided that

$$\frac{1}{4} \leqslant \frac{B_1}{B_2} \leqslant 4 \tag{26}$$

However, considering identical rotations in the walls with the above assumption, deriving the governing equation through the stationarity in the continuum model, a typical controlling parameter is defined as follows

$$\bar{\alpha}_0^2 = \frac{K_{s1}K_{s2}}{K_b(K_{s1}+K_{s2})}[(B_1+B_2)/2\ell_b+1]^2L^2 \tag{27}$$

where

$$K_b = E(I_1+I_2); \quad K_{s1} = G\kappa(A_1+A_2); \quad K_{s2} = G_{eq}t\kappa\ell_b \tag{28}$$

As stated before, this paper is devoted to study those coupled shear walls in which the connecting beams are not too stiffened. Thus, the local deformation of the walls between the beams, which occurs if the geometry of the system is getting closer to a shear-type frame, is negligible. Furthermore, it is well known that the effect of global bending is minified if the connecting beams are weaker enough than the walls. The controlling parameter can be further simplified for slender wall systems by neglecting the shear deformation in the walls ($K_{s1} \to \infty$). This is illustrated in Section 3.2 using numerical examples.

2.2.1. Application in passive damping modeling

The continuous modeling of passive dissipating devices (e.g. viscous and viscoelastic (VE) dampers [20]) in coupled shear walls can be also pursued using the present GSB. Depending on the type and distribution of devices, an equivalent dissipative core may be achieved (Fig. 4). In general, there are two common ways to place passive dampers in coupled shear walls: the vertical placement and the diagonal-braced installation.

Concerning vertical-installed devices, a damped outrigger system consisting of vertical viscous dampers was studied [42] in tall buildings using an EBB as the equivalent model and an analytical solution was developed. Lavan [19] presented shear walls coupled by diagonal-braced viscous dampers and proposed a shear damping as the equivalence of viscous dampers. He developed a continuum approach allowing a semi-analytical solution using a complex modal spectral analysis. The present GSB and its numerical solution are properly capable of overcoming the limitations (i.e. absence of shear stiffness due to smeared effect of connecting beams and the lack of a tool for damping optimization problems) of the Lavan's solution.

A schematic view of passive damper configurations and corresponding GSBs are illustrated in Fig. 4. Based on the complete or partial distribution of dampers, the continuum core may be fully or partially dissipative. Note that this study just represents the fully dissipative core systems and the partially dissipative cores and their optimization characterizations will be the subjects of an upcoming research study by the present authors.

Regarding different damper configurations, equivalent shear damping c_{eq} and stiffness k_{eq} (the stiffness is required when dealing with VE dampers) coefficients in the cores can be given by equating the energy dissipation and strain energy of the discrete model, respectively, to those of its continuum curtain. These coefficients are presented in Table 1 for the damper systems illustrated in Fig. 4. A first-order linear compatibility, as depicted in Fig. 3b, can be adopted for the rotation rates in the walls and the dissipa-tive core. A reference example is presented in Section 3.2 to ascer-tain how continuum-based models with damping can be employed to model a wall system retrofitted by viscous dampers.

2.3. The Coupled Two-Beam (CTB) model

In this section, the proposed GSB is further simplified provided that shear walls are slender enough. According to the assumption given in Eq. (26), it was demonstrated that identical rotations may be assumed in the walls (i.e. $\theta = \psi$). Therefore, a coupled shear wall can be seen such as a CTB consisting of an EBB as the con-densed effect of the walls and a RCB as the continuum core effect (see schematically the undamped CTB in Fig. 5). The equivalent rotational stiffness k_ϑ in the RCB, which depends upon G_{eq}, is defined as

$$k_\vartheta = K_{s2}\left(1+\frac{B_1+B_2}{2\ell_b}\right)^2 = G_{eq}(t\kappa\ell_b)\left(1+\frac{B_1+B_2}{2\ell_b}\right)^2 \tag{29}$$

The CTB model is governed by a single-field (u), thus, the computations can be more simplified.

It is beneficial to develop the damping models in the CTB (see damped CTB in Fig. 5). For the sake of simplicity, a unified bending damping coefficient (i.e. $c_b = c_{b1} = c_{b2}$) is assigned to the EBB. Also, an equivalent rotational (shear) damping c_ϑ can be defined in the RCB proportional to c_{eq}:

$$c_\vartheta = c_{eq}(t\kappa\ell_b)\left(1+\frac{B_1+B_2}{2\ell_b}\right)^2 \tag{30}$$

It should be remarked that the c_ϑ is employed to model both the internal viscous damping in connecting beams and the additional (external) damping. The classical viscous damping c is also introduced in the formulation (Eq. (33)).

The Total Potential Energy, Kinetic Energy, and Rayleigh Dissipation Function associated to the damped CTB are provided, respectively as follows:

$$\mathcal{V}(u) = \frac{1}{2}\int_0^L (K_b u''^2 + k_\vartheta u'^2)dx - \int_0^L qu dx \tag{31}$$

where K_b is expressed in Eq. (28).

$$T(\dot{u}) = \frac{1}{2}\int_0^L \left[\rho_d(A_1+A_2)(\dot{u})^2 + \rho_c t\ell_b(\dot{u})^2\right]dx \tag{32}$$

$$R(\dot{u}) = \frac{1}{2}\int_0^L \left[c\dot{u}^2 + c_b I(\dot{u}'')^2 + c_\vartheta(\dot{u}')^2\right]dx \tag{33}$$

Dealing with the steady-state dynamic response of the CTB system resulted by a harmonic homogeneously distributed external forcing $f(x,t) = qe^{i\omega t}$, a time-independent functional can be also introduced using Hamilton's principle. It can be easily proved that the steady state solution corresponds to the minimum of the Total Potential Energy. Separating the time-dependent and space-dependent responses, after some manipulations, stationarity gives the governing uncoupled equation of the steady-state dynamic response as:

$$K_b(1+i\omega\eta_b)u''''(x) - (k_\vartheta + i\omega c_\vartheta)u''(x) - [\omega^2(\rho_d A + \rho_c A_c) + i\omega c]u(x) = q(x) \tag{34}$$

where

$$\eta_b = c_b/E \tag{35}$$

In order to attain a benchmark for the numerical solutions in this study, the closed-form solutions of the damped CTB are presented in subsequent sections.

2.3.1. Free (complex) vibration analysis

With regard to the free vibration analysis in the complex form, substituting $q = 0$, $\omega = \omega_j$, and $u(x) = \phi_j(x)$ into Eq. (34), the corresponding expression is expressed as:

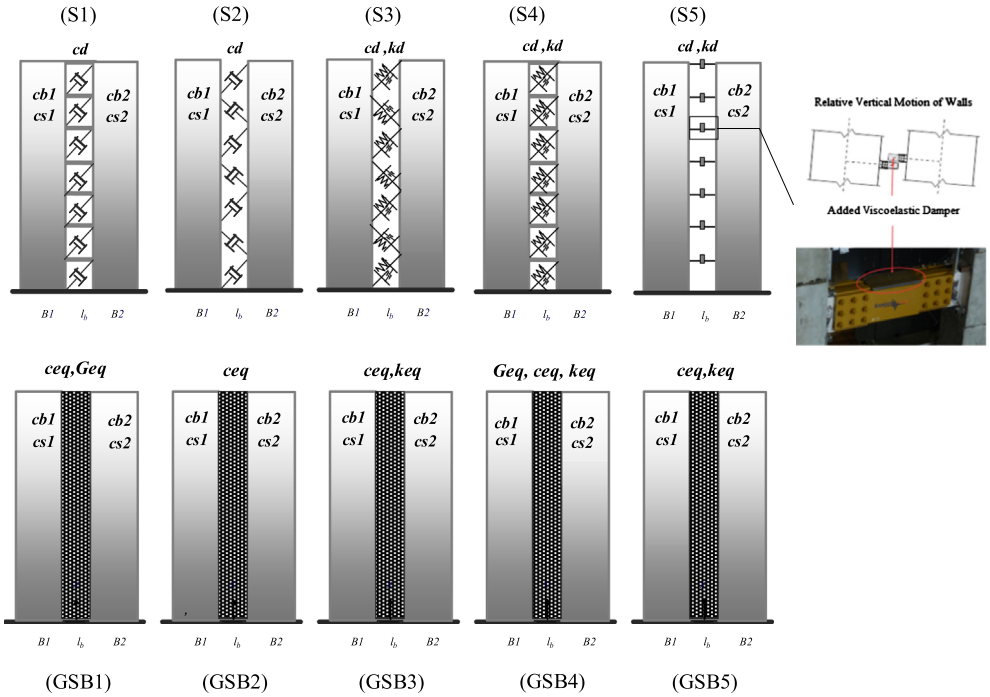

Fig. 4. Equivalent GSBs for several passive dampers: (S1) diagonal viscous dampers with connecting beams, (S2) diagonal viscous dampers without connecting beams, (S3) diagonal VE dampers without connecting beams, (S4) diagonal VE dampers with connecting beams and (S5) vertical VE dampers [20] without connecting beams.

Table 1
Equivalent stiffness and damping coefficients in GSB models.

Type of passive device	Placement direction	Equivalent stiffness k_{eq}	Equivalent damping c_{eq}
Viscous	Diagonal	–	$\frac{h\ell_b}{t(h^2+\ell_b^2)}c_d$
	Vertical	–	$\frac{\ell_b}{(ht)}c_d$
Viscoelastic (VE)	Diagonal	$\frac{h\ell_b}{t(h^2+\ell_b^2)}k_d$	$\frac{h\ell_b}{t(h^2+\ell_b^2)}c_d$
	Vertical	$\frac{\ell_b}{(ht)}k_d$	$\frac{\ell_b}{(ht)}c_d$

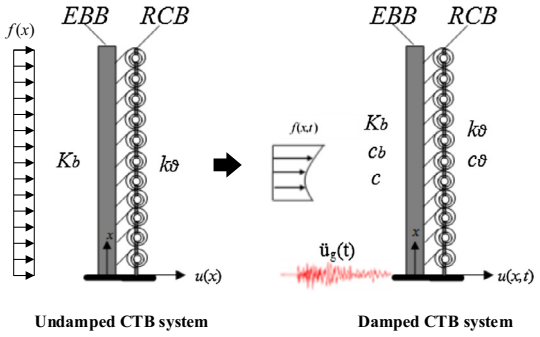

Fig. 5. Undamped and damped CTB models as parallel coupling of a condensed EBB and a rotational restraint (RCB).

$$\phi_j''''(x) - \alpha^2\phi_j''(x) - \beta^2\phi_j(x) = 0 \tag{36}$$

where

$$\alpha^2 = \frac{k_\vartheta + i\omega_j c_\vartheta}{K_b(1+i\omega_j\eta_b)}L^2; \quad \beta^2 = \frac{(\rho_d A + \rho_c A_c)\omega_j^2 + i\omega_j c}{K_b(1+i\omega_j\eta_b)}L^4 \tag{37}$$

Considering the damping effects, an analytical solution is developed by generalizing the procedure proposed [21] for the undamped CTB system. Introducing the consistent boundary conditions, the general solution of $\phi_j(x)$ can be given by

$$\phi_j(x) = \frac{\sin(\gamma_j x) - (\gamma_j/\lambda_j)\sinh(\lambda_j x) + \eta_j[\cosh(\lambda_j x) - \cos(\gamma_j x)]}{\sin(\gamma_j) - (\gamma_j/\lambda_j)\sinh(\lambda_j) + \eta_j[\cosh(\lambda_j) - \cos(\gamma_j)]} \tag{38}$$

where

$$\lambda_j = \sqrt{\alpha^2 + \gamma_j^2}; \quad \eta_j = \frac{\gamma_j^2\sin(\gamma_j) + \gamma_j\lambda_j\sinh(\lambda_j)}{\gamma_j^2\cos(\gamma_j) + \lambda_j^2\cosh(\lambda_j)} \tag{39}$$

Here, γ_j satisfies the following expression

$$\gamma_j^4 + \alpha^2\gamma_j^2 - \beta^2 = 0 \tag{40}$$

Since the latter equation is a function of the complex eigenfrequency ω_j, an additional equation is required to calculate γ_j. Therefore, applying the boundary condition corresponding to zero shear force at the top gives the new equation for computing γ_j associated with the jth mode as a function of the parameter α^2:

$$2 + \left(2 + \frac{\alpha^4}{\gamma_j^2\lambda_j^2}\right)\cos(\gamma_j)\cosh(\lambda_j) = -\frac{\alpha^2}{\gamma_j\lambda_j}\sin(\gamma_j)\sinh(\lambda_j) \tag{41}$$

With regard to Eq. (40), α^2 can be derived as the function of γ_j and be directly substituted into Eq. (41). Consequently, the eigenvalue parameter γ_j can be resulted by solving Eq. (41). To solve such a nonlinear equation, a powerful numerical solver in Mathematica® [23] has been implemented. The solution gives two values of γ_j associated to two conjugate eigenmodes. The minimum positive root corresponds to the fundamental eigenproblems, and orderly higher roots help to determine higher modes' characteristics. Note that γ_j and ω_j are both complex numbers.

Since parameters α^2 and β^2 are proportional to ω_j through Eq. (37), the conjugate eigenfrequencies of each eigenmode can be calculated on the basis of γ_j:

$$\omega_{j1,2} = \frac{-c_2 \pm i\sqrt{4c_1c_3 - c_2^2}}{2c_1} \tag{42}$$

where

$$c_1 = (\rho_d A + \rho_c A_c)L^4; \quad c_2 = \gamma_j^2\left(K_b\eta_b\gamma_j^2 + L^2 c_\vartheta - cL^4\right);$$
$$c_3 = \gamma_j^2\left(K_b\gamma_j^2 + k_\vartheta L^2\right) \tag{43}$$

The corresponding damped and free oscillating modes can be directly attained by substituting α^2 and γ_j into Eq. (38).

A suitable controlling parameter α_0^2, called the degree of coupling, is introduced based on the CTB model. This parameter is expressed where damping effects are neglected in the first expression of Eq. (37) as follows:

$$\alpha_0^2 = \frac{k_\vartheta}{K_b}L^2 \tag{44}$$

Such a parameter controls the degree of participation of overall flexural and overall shear deformations in the CTB model and thus controls the lateral deflected shape of tall coupled shear walls. A value of α_0^2 equal to zero represents a pure flexural model like an EBB (i.e. uncoupled shear walls). Such a case may be achieved where there are no connecting beams. An intermediate value of α_0^2 corresponds to the walls that combine shear and flexural deformations.

It should be noted that the parameter expressed in Eq. (44) can be straightforwardly derived through the definition of $\bar{\alpha}_0^2$ (Eq. (27)) by neglecting the walls' shear deformation (i.e. substituting $K_{s1} \to \infty$ into Eq. (27)), as it is relevant in slender systems.

2.3.2. Forced vibration analysis

Dealing now with the forced vibration, a modal analysis can be adopted [21] to obtain $u(x,t)$ in the CTB model as

$$u(x,t) = \sum_{j=1}^{n} u_j(x,t) = \sum_{j=1}^{n} \Gamma_j \phi_j(x) D_j(t)$$
$$= \sum_{j=1}^{n} \frac{\int_0^1 \phi_j(x)dx}{\int_0^1 \phi_j^2(x)dx}\phi_j(x)D_j(t) \tag{45}$$

where $D_j(t)$ associated to each mode can be derived by solving the following equation

$$\ddot{D}_j(t) + 2\zeta_j\omega_j\dot{D}_j(t) + \omega_j^2 D_j(t) = \begin{cases} -\ddot{u}_g(t): \text{ Ground Acceleration} \\ f(t)/m_j: \text{ Harmonic Excitation} \end{cases} \tag{46}$$

The influence of various damping models must be taken into account for the evaluation of $D_j(t)$. The modal damping factor ζ_j can be obtained from Eq. (17), while those related to higher modes are also allowed. Depending on the type of the damping mechanism, the level of ζ_j in each mode may be different. This point is discussed in numerical sections.

The inter-story drift ratio, $IDR(x,t)$, is an important measure of nonstructural damage and can be evaluated by the derivative of the displacement:

$$IDR(x,t) = \frac{\partial u(x,t)}{\partial x} = \frac{1}{L}\sum_{j=1}^{n} \Gamma_j \phi_j'(x) D_j(t)$$
$$= \frac{1}{L}\sum_{j=1}^{n} \frac{\int_0^1 \phi_j(x)dx}{\int_0^1 \phi_j^2(x)dx}\phi_j'(x)D_j(t) \tag{47}$$

The absolute acceleration, when the system is subjected to a ground motion, is a measure of damage to nonstructural acceleration sensitive equipment as well as contents' movement along the floor area

$$\ddot{u}^t(x,t) = \ddot{u}_g(t) + \sum_{j=1}^{n} \Gamma_j \phi_j(x)\ddot{D}_j(t)$$
$$= \ddot{u}_g(t) + \sum_{j=1}^{n} \frac{\int_0^1 \phi_j(x)dx}{\int_0^1 \phi_j^2(x)dx}\phi_j(x)\ddot{D}_j(t) \tag{48}$$

Time-dependent bending moment $M(x,t)$ reads

$$M(x,t) = \sum_{j=1}^{n} M_j(x,t) = \sum_{j=1}^{n} \Gamma_j\left[K_b\int_x^1 \phi_j''(x)dx - k_\vartheta\int_x^1 \phi(x)dx\right]D_j(t) \tag{49}$$

and shear force $V(x,t)$ is given by

$$V(x,t) = \sum_{j=1}^{n} V_j(x,t) = \sum_{j=1}^{n} \Gamma_j\left[K_b\int_x^1 \phi_j'''(x)dx - k_\vartheta\int_x^1 \phi_j'(x)dx\right]D_j(t) \tag{50}$$

The base overturning moment and the base shear time-histories are expressed in Appendix C. It should be remarked that the effect of different damping mechanisms is included in $D_j(t)$ expressed in Eq. (46).

3. Results and discussions

3.1. Verification of undamped RB model

A set of verifications has been accomplished to verify the FEM developed for the RB. For this purpose, an asymmetrical coupled shear walls system [25] is considered (see Fig. 6). The effectiveness of the present FEM is demonstrated with regard to static and free vibration problems by comparison with the results of a FEM software SAP2000, whereas all the structural members are modeled by shell elements. The first four natural frequencies are calculated using the proposed FE model and compared (see Table 2), respectively, to those found in the literature Takabatake [25] and those computed by SAP2000; the results are found to be in agreement with the maximum error less than 5%. It should be noted that a length magnification factor, $\varepsilon = 1/12$, is adopted to take into account the deformation in junctions. The static tip displacement is also compared (Table 2) with those resulting from other meth-ods, therein showing a lower response with respect to the solution obtained from SAP2000 model and a higher one compared to the solution of Takabatake [25].

3.2. Verification of damped RB, GSB, and CTB

In this section, the verification of the three damped beam systems (i.e. RB, GSB, and CTB) is addressed. It is assumed that the reference example is subjected to the given harmonic load $f(t)$ = 16,500 $\sin(0.9\omega_1 t)$ which is uniformly distributed. Two damping mechanisms are considered to provide totally 5% damping ratio in the fundamental mode. The damping mechanisms, which are adopted in the RB model, are: (1) $\eta_{b1} = \eta_{b2} = 0.01$ in the main beams and (2) $\eta_{b3} = 0.002$ in the set of connecting beams. Note that only the internal bending damping is taken into account because of its dominant efficiency in contrast to the shear damping.

Using Eq. (27), the controlling parameter $\bar{\alpha}_0^2 = 7.25$ on the basis of the GSB is attained. Meanwhile, $\alpha_0^2 = 7.9$ with the CTB model is calculated through Eq. (44), showing that the difference between $\bar{\alpha}_0^2$ and α_0^2 in tall structures is not significant. For the GSB system, the equivalent damping in the continuum core, $c_{eq} = 9.59\times 10^5$ N s/m^2, is found through the first expression of Eq. (24). The corresponding rotational (shear) damping in the CTB model,

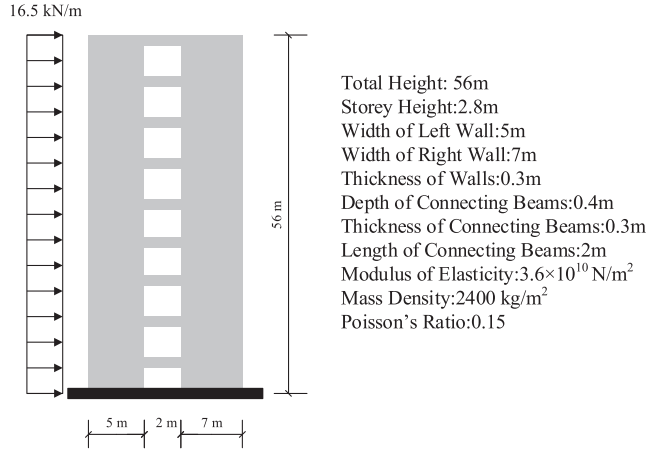

Fig. 6. An asymmetrical coupled shear walls system [25].

Table 2
Tip displacement and natural frequencies with the benchmark and RB model.

Reference model	Tip displacement (m)	Natural frequency (Hz)			
		Mode 1	Mode 2	Mode 3	Mode 4
RB	0.0161	13.06	54.17	128.17	227.13
SAP2000	0.0165	13.01	53.55	126.24	223.60
Takabatake [25]	0.0158	13.09	55.55	129.00	224.90

$c_\vartheta = 5.67 \times 10^6$ N s, can be obtained with Eq. (30). The dynamic tip displacements resulted by the three models are shown in Fig. 7. It can be seen from Fig. 7 that the three models give almost identical responses with good agreements in the general features of time histories. Note that the contribution of first three modes is considered to obtain the solution of CTB using Eq. (45).

Other dynamic responses such as first three damped eigenfrequencies, first damping factor ζ_1, peak displacement u_{max}, maximum inter-story drift ratio IDR_{max}, peck base moment $M_{b,max}$, and maximum base shear $V_{b,max}$ are also evaluated by the three beam systems and presented in Table 3. According to this table, all the responses are in acceptable agreements.

In addition to the present benchmark (Fig. 6), a 13-story RC shear wall structure [19] is also analyzed. It is required to retrofit the building, since the walls are not able to resist the resulting moment at the base. Viscous dampers are thus installed diagonally between the walls. The building is excited by the LA07 ground motion. The details about this structure can be found in the litera-ture [19]. The GSB2, which corresponds to the present example and is illustrated in Fig. 4, is selected. The damping coefficient provided by viscous dampers is c_d = 3425 kN s/m, thus, the equivalent core shear damping c_{eq} = 19,000 kN s/m^2 is obtained through the expression proposed for diagonal viscous dampers (see Table 1). Moreover, on the basis of the GSB2, a CTB model is correspondingly defined and the rotational (shear) damping c_ϑ = 128,000 kN s is obtained from Eq. (30). The controlling parameters are based on
the both GSB and CTB are equal $\bar{\alpha}_0^2 = \alpha_0^2 = 0$. Table 4 presents important structural responses found in the literature [19] and those computed by the continuum-based models and the discrete model using the software SAP2000. The viscous dampers are modeled with linear damper-type link elements in the SAP2000. It should be remarked that the shear damping is considered in this investigation, hence, the bending and classical damping effects are neglected. Comparing the results of continuum-based models and those obtained from the discrete system reveals that the present models are reliable.

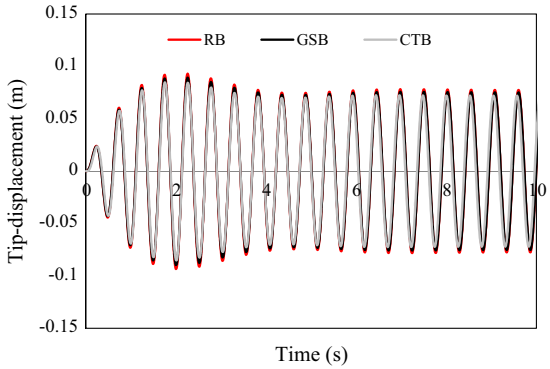

Fig. 7. Tip displacement oscillation resulted by damped RB, GSB, and CTB.

3.3. Eigenfrequency properties influenced by DIVD in connecting beams

The properties of fundamental complex eigenfrequency ω_1 of the reference system (Fig. 6) are shown (Fig. 8a–d) with regard to bending η_b and shear η_s damping multipliers in connecting beams. The RB model is used to analyze the problem. It can be observed from Fig. 8a that the oscillation part of ω_1 is identical by both damping mechanisms with no sensible variation up to a certain damping multiplier ($\eta_b = \eta_s = 0.05$). Fig. 8b indicates the magnified view of the diagrams shown in Fig. 8a along very small damping multipliers. The oscillating part influenced by the bend-ing damping dramatically grows up at $\eta_b = 0.16$, meaning that a sharp change is occurred from the flexural mode in connecting beams to the shear mode. The diagram finally tends to a stable branch with the oscillating part equal to 63.5 Hz. At this level, the internal bending damping has damped out the flexural vibra-tion in the set of connecting beams. Comparing the influence of bending and shear damping models in the present coupling beams, it can be understood that the bending damping mechanism is more efficient than the shear one.

The damping part of ω_1 is also shown in Fig. 8c. It can be seen that the damping part influenced by the bending damping is a diagram with a single peck. This diagram gives the optimum damping multiplier $\eta_b = 0.2$ resulting in the decay rate of of 40 Hz. The diagram resulted by the shear damping (dashed line in Fig. 8c) has an almost linear trend with considerably lower values. It strongly confirms that the bending damping is dominant in the reference connecting beams in comparison with the shear one. The first modal damping ratio ζ_1 produced by both damping mechanisms is estimated (Fig. 8d) through Eq. (17) for small damping multipliers. It can be seen from Fig. 8d that both diagrams vary almost linearly, but the ratio provided by the bending damping is dominantly significant in contrast to the one resulted by the shear damping.

3.4. Eigenfrequency properties influenced by DIVD in main beams (walls)

In order to realize the performance of each damping mechanism (i.e. bending and shear damping) in the walls against the classical viscous damping in the reference structure, the oscillating and damping parts of ω_1 are evaluated by the RB model versus corresponding damping factors (see Fig. 9a and b, respectively). It should be noted that the bending and shear damping coefficients are assumed identical in the both (walls) main beams (i.e. $c_{b1} = c_{b2}$ and $c_{s1} = c_{s2}$). Concerning the oscillating part, which is normalized with respect to the undamped natural frequency, all the three damping mechanisms cause almost the same amount up to about 15% of critical damping, meaning that there is no behavioral

Table 3
First three damped eigenfrequencies and dynamical responses by the RB models.

Model	ω_1	ω_2	ω_3	ζ_1	u_{max} (m)	IDR_{max}	$M_{b,max}$ (ton m)	$V_{b,max}$ (ton)
RB	$-0.67 + 13.35i$	$-14.37 + 55.19i$	$-96.37 + 104.4i$	0.05	0.093	0.0021	70,725	3810
GSB	$-0.69 + 13.29i$	$-14.27 + 54.56i$	$-94.13 + 103.6i$	0.052	0.0895	0.002	68,631	3758
CTB	$-0.73 + 13.35i$	$-14.93 + 55.1i$	$-99.33 + 103.3i$	0.0546	0.085	0.00195	72,850	3897

Table 4
Structural responses by different models, obtained for both 5% inherent damping and additional (viscous) damping.

Damping sort	5% inherent damping			Passive damping (viscous damper)				
				Discrete approach		Continuous approach		
Response	Lavan [19]	GSB	CTB	Lavan [19]	SAP2000	Lavan [19]	GSB	CTB
Natural period (s)	3.69	3.69	3.69	–	–	3.74	3.6	3.59
Damping ratio of first mode	0.05	0.05	0.05	–	–	0.266	0.263	0.267
Roof displacement (m)	0.386	0.387	0.4	0.165	0.162	0.163	0.172	0.176
Max. inter-story drift ratio (%)	1.37	1.36	1.35	0.62	0.6	0.58	0.46	0.52
Max. absolute acceleration (m/s^2)	8.21	7.26	7.12	4.38	4.86	5.55	4.72	4.53
Total base shear (kN)	9453	9598	9635	5620	5360	5014	6139	6228
Total base moment (kN m)	230,600	229,000	238,000	126,000	121,000	113,600	112,000	114,400

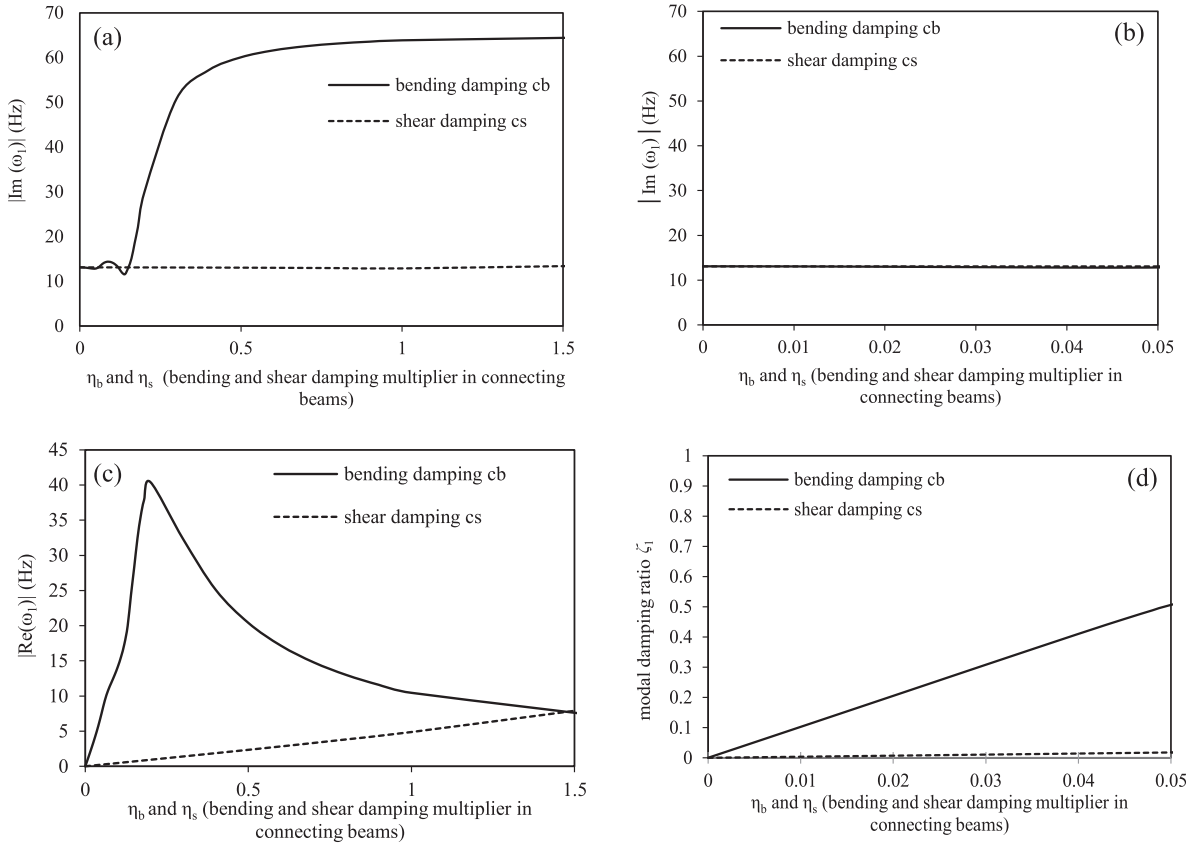

Fig. 8. Fundamental eigenfrequency characteristics of the reference structure including (a) trend of oscillating part, (b) zoomed in view of oscillating part associated to small multipliers, (c) trend of damping part and (d) trend of modal damping ratio ζ_1 versus damping multipliers.

difference by employing each damping mechanism. According to Fig. 9a, the curve related to the internal shear damping slightly alters the oscillating part up to 13.35 Hz, confirming that the shear oscillation is completely destroyed and walls vibrate only flexurally. However, the shear damping in the walls of such a case study structure is not so efficient. Fig. 9a clearly shows that both internal bending and classical viscous damping are able to damp out properly the oscillating part of ω_1. Note that when the oscillating part is vanished, then the critical damping is achieved.

With regard to the damping part (Fig. 9b), the curve associated to the classical damping linearly varies up to the critical value. According to Fig. 9b, there is an overlap between the diagrams by the classical and bending damping for damping factors less than 0.2. For damping factors greater than 0.2, the bending damping

enforces higher damping parts in comparison with the classical damping and finally reaches the critical level at 17.89 Hz. The critical value produced by the classical damping is 13.06 Hz. It can be also mentioned that the damping part influenced by the shear damping is negligible in contrast to the other damping models (see Fig. 9b).

3.5. Effects of damping mechanisms and degree of coupling on structural characteristics

Various damping systems (bending, classical, and shear damping) can be used to model the dissipation mechanism in coupled shear walls. In order to better realize which damping mechanism is more efficient in slender systems, some numerical investigations are carried out. It should be noted that the degree of coupling (Eq. (44)) is utilized instead of the controlling parameter expressed in Eq. (27), whereas the walls are assumed slender enough. Moreover, the bending damping coefficients in the walls are assumed identical (i.e. $c_{b1} = c_{b2} = c_b$). Critical damping values versus the degree of coupling α_0^2 are plotted corresponding to the bending and classical damping and are shown in Fig. 10a and b, respectively. The both damping models are assumed uniformly distributed along the system. It can be observed from the graphs of Fig. 10 that larger degrees of coupling result in higher critical damping values. Note that the first study is devoted to the bending and classical damping and the results on the shear damping are later explained. For the sake of simplicity, a damping factor $\zeta = c/c_{cr} = \eta_b/\eta_{b,cr} = c_v/c_{v,cr}$ associated to the first mode is defined in order to be able to equally compare the dynamic characteristics by the damping models.

Having assumed different values of the degree of coupling, e.g. $\alpha_0^2 = 0$; $\alpha_0^2 = 6$; $\alpha_0^2 = 25$; $\alpha_0^2 = 100$, the trend of $Im(\omega_1)$ of the fundamental eigenfrequency ω_1 influenced by the classical and bending damping is shown in Fig. 11a–d, respectively. As it can be seen from the graphs of Fig. 11, the oscillating parts influenced by the damping models incrementally diverge where α_0^2 increases. For the both damping cases, the oscillating part becomes zero at the critical level (i.e. $\zeta = 1$). According to Fig. 11a, the influence of the damping models is almost identical for $\alpha_0^2 = 0$ (uncoupled shear walls). According to Fig. 11a–c, the same performance can be seen with low damping factors for the bending and classical damping models.

Furthermore, the tendency of absolute damping part $|Re(\omega_1)|$ with different degrees of coupling is plotted in Fig. 12a–d. Concerning $\alpha_0^2 = 0$, the damping part affected by the both damping systems varies almost linearly (Fig. 12a). Increasing α_0^2, the diagrams associated to the bending damping gradually become nonlinear, especially for damping factors less than about 0.3. According to the plots shown in Fig. 12, the bending damping exhibits significantly higher damping part for larger α_0^2 in comparison with the classical damping.

For a better understanding, the ratio of $Re(\omega_1)$ resulted by the bending and classical damping is plotted (Fig. 13a) versus α_0^2 for $\zeta < 0.2$. For very small α_0^2, Fig. 13a shows that the ratio approaches 1 by increasing the ζ. This ratio is signified, when ζ decreases and α_0^2 increases.

A suitable performance index, the Inter-story Drift Transfer Function (IDTF) [43], is also selected to compare the efficiency of the damping mechanisms. For this purpose, the ratio of sum of IDTF in the system resulted by the two damping models is plotted (Fig. 13b) against the α_0^2; the index ratio is generally reduced by magnifying α_0^2. This reduction is more significant for smaller ζ, indicating that the bending damping is more effective than the classical damping for mitigating the sum of IDTF. Note that both damping models perform similarly when the degree of coupling tends to zero (see Fig. 13b).

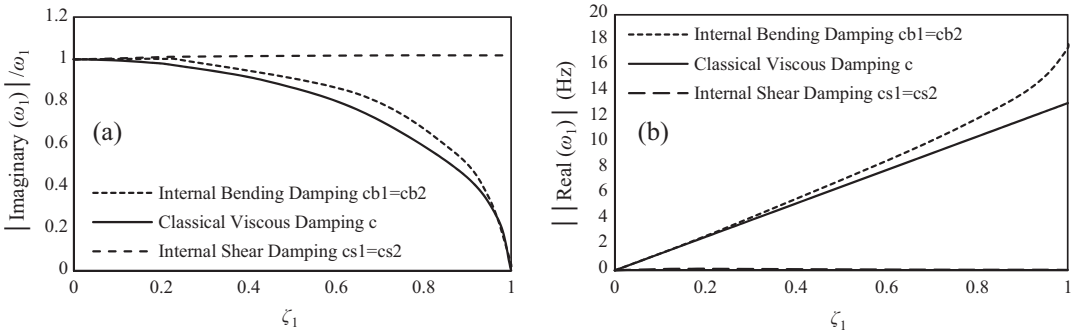

Fig. 9. Trend of (a) normalized oscillating part and (b) damping part of ω_1 versus different damping factors resulted by internal bending and shear damping in walls and the classical damping.

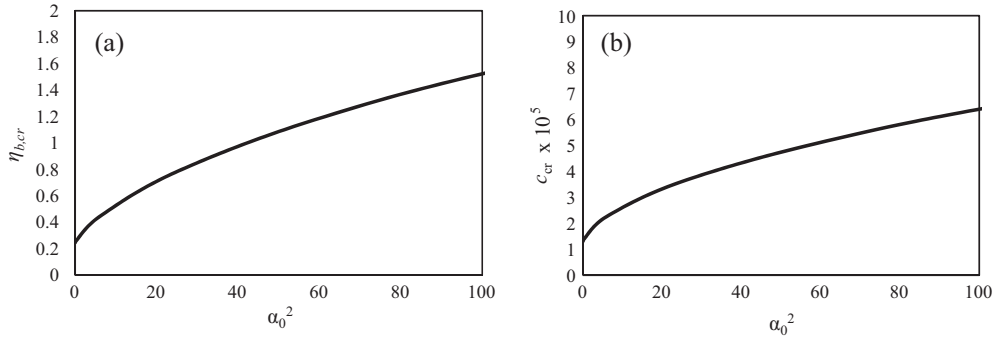

Fig. 10. Critical values of (a) internal bending damping multiplier and (b) classical damping versus the degree of coupling α_0^2.

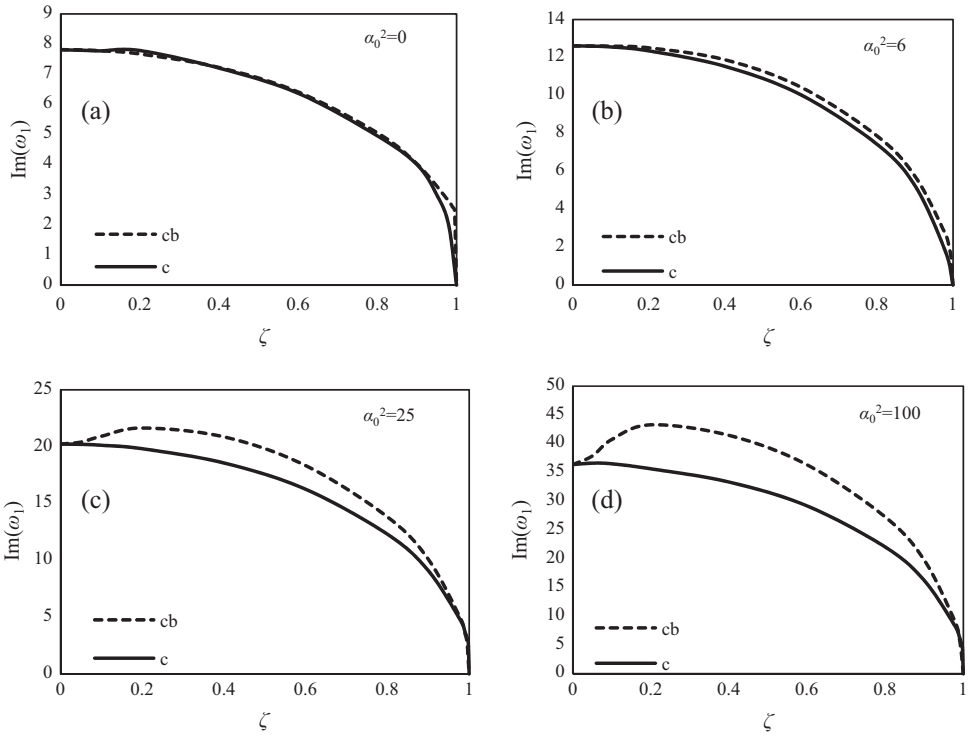

Fig. 11. Dependency of frequencies of freely oscillating CTB with respect to bending and classical damping coefficients for several degrees of coupling (a) $\alpha_0^2 = 0$, (b) $\alpha_0^2 = 6$, (c) $\alpha_0^2 = 25$ and (d) $\alpha_0^2 = 100$.

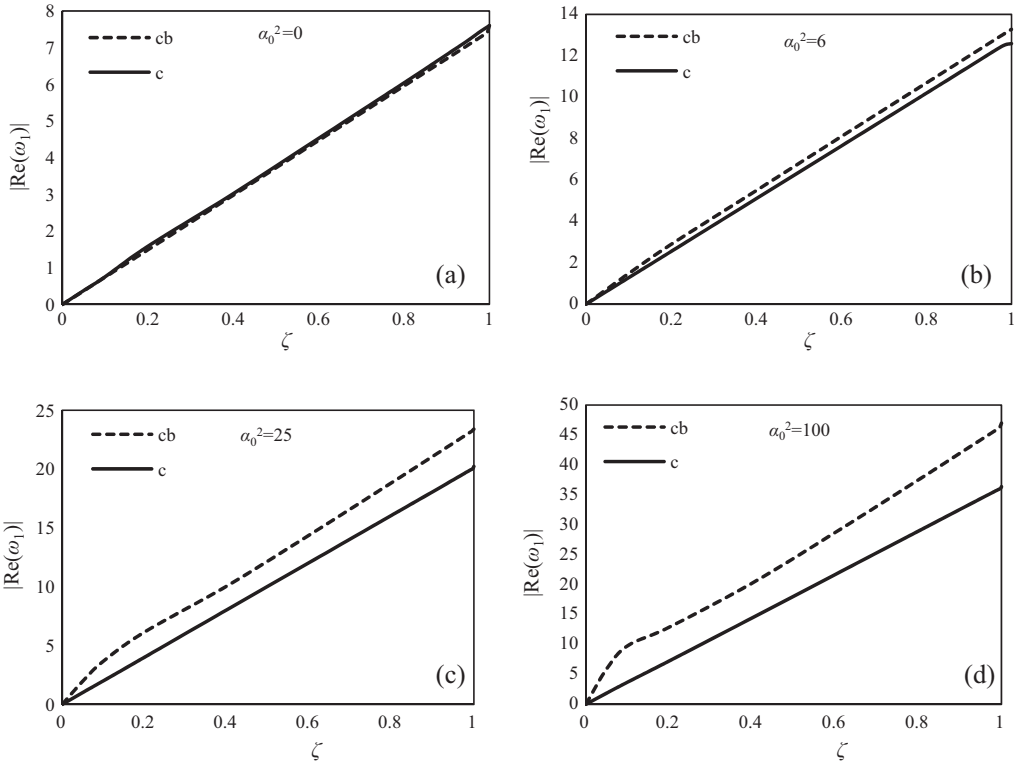

Fig. 12. Decay rate of the free oscillating CTB system increasing bending and classical damping coefficients for several degrees of coupling (a) $\alpha_0^2 = 0$, (b) $\alpha_0^2 = 6$, (c) $\alpha_0^2 = 25$ and (d) $\alpha_0^2 = 100$.

In addition to the damped free vibration, the forced responses are moreover studied to ascertain the inherent characteristics of the damping models. Hence, the ratio of tip displacement Dynamic Magnification Factor (DMF) and the maximum inter-story drift ratio (IDR_{max}) are plotted in Fig. 14a and b, respectively; various degrees of coupling limited by $0 \leqslant \alpha_0^2 \leqslant 100$ are considered. Note that a uniformly distributed harmonic force with excitation frequency equal to the fundamental frequency (i.e. $\omega = \omega_1$) is adopted

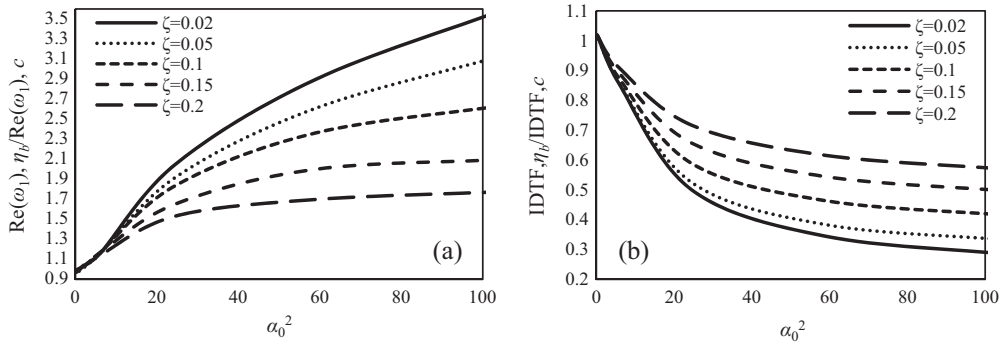

Fig. 13. Ratio of (a) decay rate and (b) sum of IDTF by bending and classical damping with respect to α_0^2 for various damping factors.

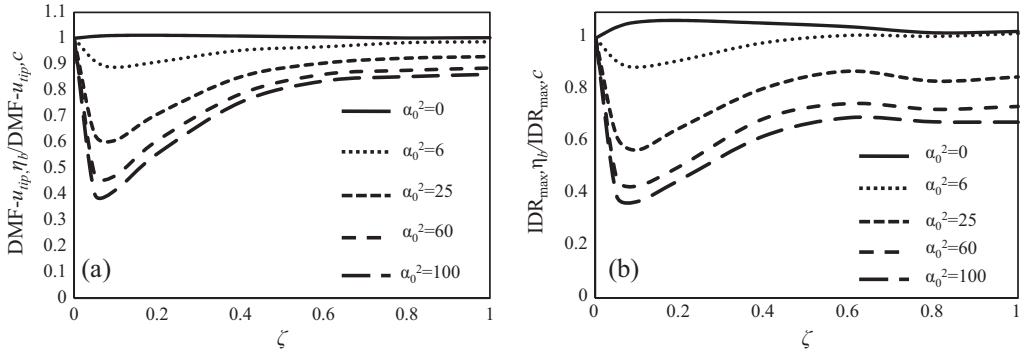

Fig. 14. Ratio of (a) dynamic magnification factor (DMF) of tip displacement u_{tip} and (b) maximum inter-story drift ratio (IDR_{max}) in damped CTB systems by bending and classical damping for different α_0^2 with respect to damping factors ζ.

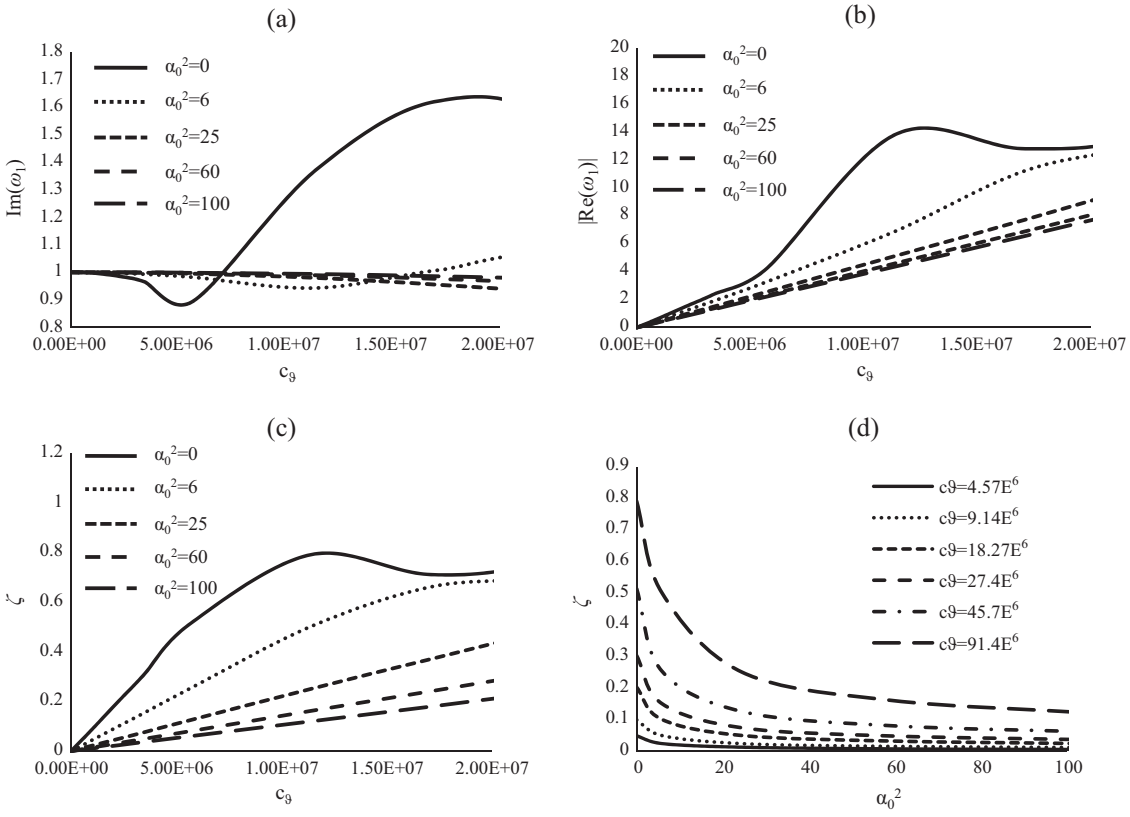

Fig. 15. Influence of distributed rotational (shear) damping c_ϑ on (a) free oscillating part, (b) decay rate (damping) part and (c and d) damping factor ζ with respect to the coupling degree α_0^2.

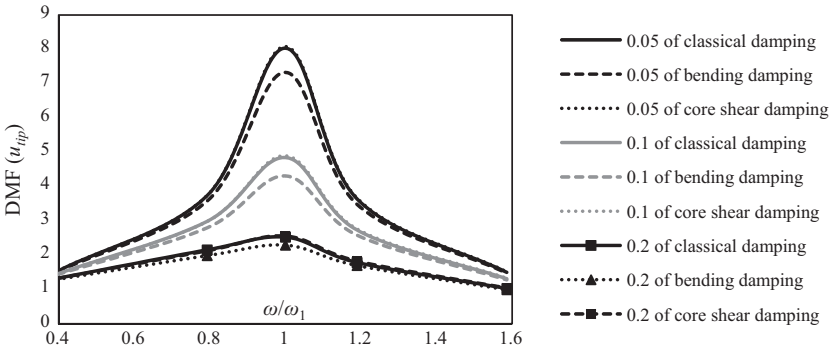

Fig. 16. Transfer function of tip displacement u_{tip} in the reference structure $\bar{\alpha}_0^2 = 7.25$ by classical, bending, and core shear damping models.

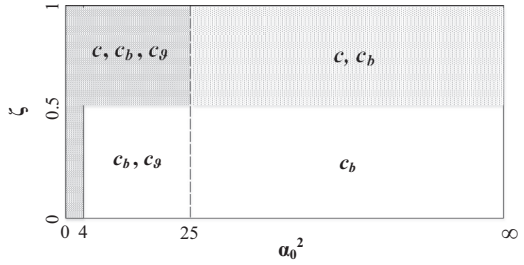

Fig. 17. Qualitative scheme for the optimal damping model to be used for different degrees of coupling α_0^2 and damping factors ζ adopted in coupled shear walls.

for analysis. It can be seen from the both plots of Fig. 14 that the response ratios are smaller especially for $0.03 \leqslant \zeta \leqslant 0.6$ and larger degrees of coupling (e.g. $\alpha_0^2 = 60, 100$). In the same range of damping factors, the ratio of DMF approaches about 1 by decreasing the α_0^2 (see Fig. 14a). For $\zeta > 0.6$ and every α_0^2, the response ratio is almost stable. The graph presented for the IDR_{max} (Fig. 14b) indicates almost similar trends to the one shown in Fig. 14a.

The rotational (shear) damping mechanism c_ϑ, which is applied to model both inherent and additional damping through the CTB model, is also evaluated; the oscillating part, damping part, and damping factor ζ are represented 9 Fig. 15a–d for various values of α_0^2. Fig. 15a and b shows that the systems with smaller α_0^2 are more sensitive to the variation in c_ϑ. This sensitivity is more dominant for the uncoupled shear walls ($\alpha_0^2 = 0$). According to Fig. 15b, the damping parts in systems with greater α_0^2 vary almost linearly and exhibit lower values in contrast to those with smaller α_0^2. Fig. 15c clearly indicates that the damping factors provided by c_ϑ are dominant in the systems with smaller α_0^2. In order to better understand the variation of overall damping with respect to α_0^2, Fig. 15d is represented for several shear damping values c_ϑ; less damping factors are always obtained by increasing α_0^2. To achieve higher damping values with a certain c_ϑ, small or moderate degrees of coupling are desirable; such a case may be attained by designing flexible enough connecting beams in coupled shear walls.

Concerning the reference example (Fig. 6), the influence of the classical, internal bending, and shear damping models are independently analyzed on the tip displacement transfer function (DMF) (see Fig. 16). Three damping ratios (0.05, 0.1, and 0.2) associated to the fundamental mode are taken into consideration. It can be observed form Fig. 16 that the classical and shear damping cause almost the same response with the same damping factor, while the bending damping exhibits a lower level of transfer function, especially around $\omega/\omega_1 = 1$. Note that the behavior of the damping models may be different in higher modes.

Based upon the comprehensive investigations on various structural characteristics, a general framework is finally proposed for selecting suitable damping mechanisms in coupled shear walls (see Fig. 17). This framework is dependent upon two key parame-ters: the degree of coupling α_0^2 and the damping factor ζ. According to the present framework, the shear-type damping c_ϑ is appropri-ate to model passive damping effects (e.g. viscous and viscoelastic devices) in systems with lower degrees of coupling (e.g. $\alpha_0^2 < 25$). In general, larger α_0^2 causes lower damping amounts by the shear damping c_ϑ. Fig. 17 illustrates that the bending damping c_b in

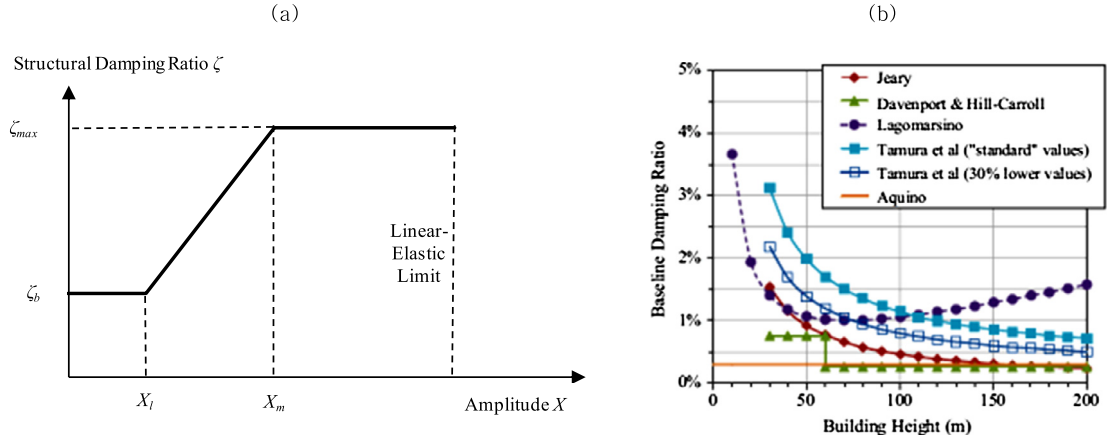

Fig. 18. (a) General shape of current damping predictor models. (b) Baseline damping ratios, assigned to the low-amplitude plateau, suggested in different literatures as the possible damping predictor model for safety design under wind loads [54].

Table 5
Baseline damping proposals intended for the wind-resistant design.

Reference	Baseline damping ratio ζ_b
Jeary [46]	$0.01f \cong 0.46/L$
Lagomarsino [50]	$\beta_1 f + \beta_2/f$
Tamura et al. [51,52]	$\gamma_1 f + \gamma_2 \cong \gamma_3/L + \gamma_2$

f: natural frequency; L: building height; β_1, β_2, γ_1, γ_2, γ_3: parameters dependent upon primary construction material.

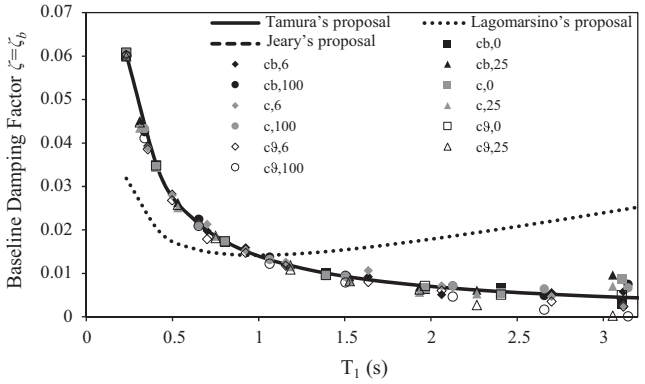

Fig. 19. Comparison of baseline (fundamental) damping with three damping mechanisms and proposed predictors presented in Table 5.

coupled walls is the most suitable model and is applicable for every range of α_0^2 and ζ. Such a damping mechanism is generally suggested as the inherent damping. In addition, an external bending damping might be developed, where damped outrigger systems are installed in tall buildings supported by shear walls [44]. Concerning large α_0^2, the bending damping c_b is still more suitable than the classical damping c. This priority is more significant especially when lower damping factors ($\zeta < 0.5$) are required (see the portion surrounded by $\zeta = 0.5$ and $\alpha_0^2 = 25$ in Fig. 17). For higher damping factors (e.g. $\zeta > 0.5$), both bending c_b and classical c damping models may be adopted with almost identical behavior. According to Fig. 17, provided that $\alpha_0^2 > 4$ and $\zeta < 0.5$, the bending damping c_b is yet preferred in comparison with the classical damping c.

3.6. Suitability of damping mechanisms for wind-based damping models

It has been demonstrated [45–47] that a significant portion of overall damping in RC buildings in small displacement amplitudes is material damping. This point prompted the present authors to investigate also the suitability of the classical damping and proposed DIVD models (i.e. internal bending and shear damping) for inherent damping modeling via continuous beam systems. Given the importance of damping in the wind-resistant design of buildings, compatibility of proposed damping mechanisms with the current structural damping models (Fig. 18a) reported in the literature (Jeary [46,48,49], Lagomarsino [50], Tamura [51], and Spence and Kareem [53]) is studied. For the first constant part of the current models (see Fig. 18a), called *baseline damping ratio* ζ_b, some proposals are listed in Table 5. The ζ_b versus the building height based on these proposals is also shown in Fig. 18b. Note that the amplitude-dependent part of the damping predictor models is not the subject of this study.

A comparative investigation is carried out (Fig. 19) between the models presented in Table 5 and the fundamental (baseline) damping ratio resulted by the three damping mechanisms (bending c_b, classical c, and shear damping c_ϑ) and using degrees of coupling α_0^2 = 0, 6, 25, 100. As it can be seen from Fig. 19, the trend of damping ratio provided by all the damping mechanisms and degrees of

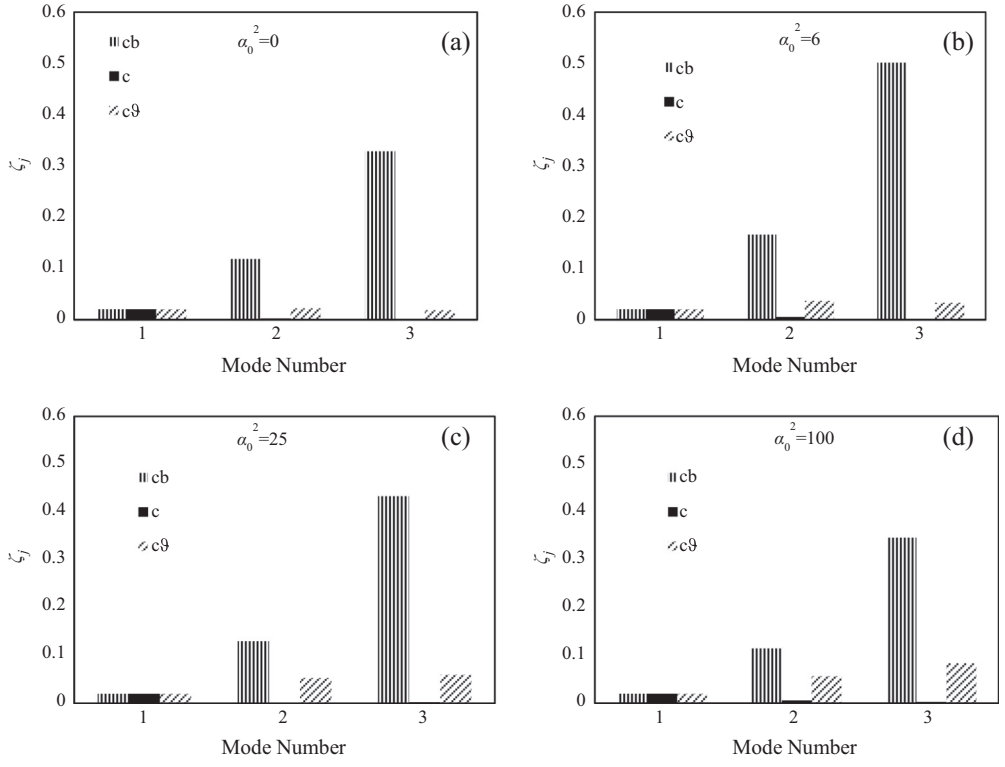

Fig. 20. Identification of modal damping ratios ζ_j provided by internal bending c_b, classical c, and rotational (shear) c_ϑ damping for (a) α_0^2 = 0, (b) α_0^2 = 6, (c) α_0^2 = 25 and (d) α_0^2 = 100.

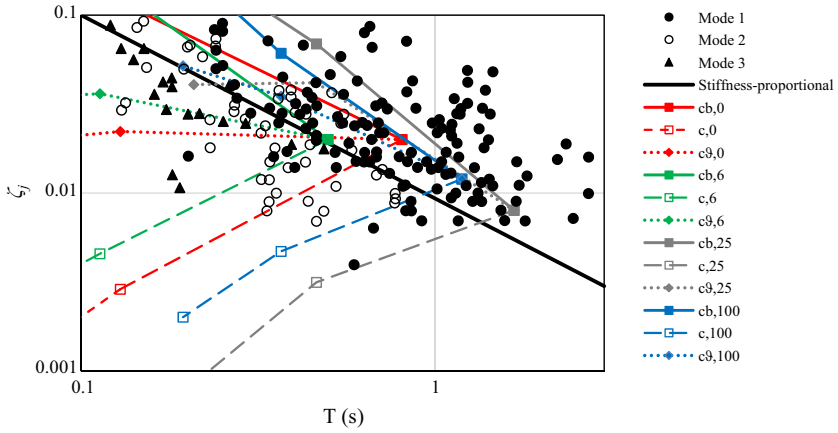

Fig. 21. Comparison of modal damping ratio trend with different damping models and degrees of coupling (e.g. $\alpha_0^2 = 0, 6, 25, 100$) against measured data for Japanese RC buildings [45] in the first three modes.

coupling is considerably in agreement with Tamura's model (i.e. $\zeta_b = 0.014/T_1$). There are slight differences for higher periods (e.g. $T_1 > 3$ s) corresponding to very tall systems. According to Fig. 19, the Jeary's proposal (i.e. $\zeta_b = 0.01/T_1$) is less in agreement with the damping ratios resulted by the present damping models. Also, the damping ratios obtained from the Lagomarsiono's model is different from the other results (see Fig. 19).

Damping ratios in higher modes ζ_j (j = 2,3) are also evaluated (see Fig. 20) using the proposed damping mechanisms. Depending upon every α_0^2, certain quantities of coefficients c, c_b, and c_ϑ are selected in such a way to obtain the same damping $\zeta_1 = \zeta_b = 0.02$ in the fundamental mode estimated through the Tamura's model with the height of 56 m (refer to Fig. 18b). Then, it can be realized how much damping will be provided in the second and third modes using the achieved damping coefficients (see Fig. 20). It can be clearly observed from Fig. 20 that the bending damping c_b supplies significant damping in higher modes; the damping ratios in higher modes resulted by the classical damping c are very low in comparison with those obtained with the other damping models. Fig. 20a shows that the shear (rotational) damping c_ϑ provides almost identical modal damping ratios, where $\alpha_0^2 = 0$ and gives larger ratios in higher modes by magnifying α_0^2 (see Fig. 20c and d).

Given the eligibility of bending and shear damping in higher modes, the compatibility of the damping models against the full-scale data measured [45] in the first three modes of Japanese RC buildings is also addressed (see Fig. 21). Selecting aforementioned degrees of coupling α_0^2 and fundamental natural periods T_1, the damping ratio in the first mode is identically fixed with all the three damping mechanisms (i.e. c, c_b, and c_ϑ) using the Tamura's proposal (i.e. $\zeta_1 = 0.014/T_1$). It can be seen from Fig. 21 that as the period T becomes smaller (i.e. the modal number becomes higher), the measured damping ratios are increasing. Damping ratios caused by the stiffness-proportional type damping (filled black line in Fig. 21) and the bending damping (filled lines with markers in Fig. 21) are also increasing, but the rates of increment are higher than the measured data with the both cases. Fig. 21 shows that the classical damping (dashed lines in Fig. 21) is inca-pable of modeling the full-scale data, since damping ratios are reducing as the period T decreases. According to Fig. 21, the varia-tion of damping ratio by the shear damping (dotted lines in Fig. 21) is almost in agreement with the full-scale measurements. How-ever, it can be concluded that DIVD models classified into bending and shear mechanisms give much closer results to the real data, while the classical damping is suitable only in the fundamental mode. Note that a hybrid damping consisting of bending c_b and shear c_ϑ damping may approximate more accurately the real measurements; moreover, the amplitude-dependent range of the structural damping (see Fig. 18a) may be analyzed using such a damping model. The latter goal can be afforded since the bending and shear damping, which are basically viscoelastic models (Eq. (5)), are prone to be altered depending on the level of strain; while the linear classical damping is incapable in this case.

4. Conclusions

This study is devoted to develop relevant viscous damping models through multi-beam systems in coupled shear walls consisting of weak connecting beams compared to the walls. For this purpose, in addition to the linear classical viscous damping, the Distributed Internal Viscous Damping (DIVD) composed by the bending and shear mechanisms is introduced through three beam systems: Reference Beam (RB), Generalized Sandwich Beam (GSB), and Coupled Two-Beam (CTB). A low-order FE model used to facilitate the dynamic analysis is developed for the first two systems and the third system is solved analytically. Useful (shear-type) continuum-based coefficients are presented to equivalently analyze the performances of passive dampers; hence, the seismic analysis of a retrofitted structure numerically revealed the suitability of such a technique in modeling of diagonal-braced viscous dampers via the GSB and CTB systems.

The numerical analysis of the reference example using the RB showed that the bending damping in both the walls and coupling elements is dominant against the shear damping. Employing the GSB and two controlling parameters called the *degree of coupling* and the *damping factor* associated to the fundamental mode, some structural characteristics are comparatively investigated with the classical damping and DIVD models, indicating that the bending damping is the most efficient mechanism with every degree of coupling. The investigations showed that the classical damping behaves almost identical to the bending and shear damping for degrees of coupling less than 4 and is not suitable with larger degrees of coupling than this value and small damping factors. The shear-type damping, which is proposed as the continuous (smeared) equivalence of internal damping in ordinary connecting beams and of the additional (passive) coupling devices, is identified to be more efficient with degrees of coupling less than about 25. Numerical investigations also revealed that the bending damping in the walls and shear damping in the core (smeared coupling elements) are suitable not only in fundamental mode but also in higher modes, since they render closer damping ratios to the measured data given for RC buildings against the classical damping.

Appendix A

The FE mass matrix M_e determined for the RB system reads:

$$M_e = \frac{\rho\ell}{6}\begin{bmatrix} 2(A_1+A_2) & 0 & 0 & (A_1+A_2) & 0 & 0 \\ 0 & 2I_1 & 0 & 0 & I_1 & 0 \\ 0 & 0 & 2I_2 & 0 & 0 & I_2 \\ (A_1+A_2) & 0 & 0 & 2(A_1+A_2) & 0 & 0 \\ 0 & I_1 & 0 & 0 & 2I_1 & 0 \\ 0 & 0 & I_2 & 0 & 0 & 2I_2 \end{bmatrix} \tag{A.1}$$

The FE stiffness matrix K_e of the RB is expressed as

$$K_e = \frac{1}{2\ell}\begin{bmatrix} 2(K_{s1}+K_{s2}) & K_{s1}\cdot\ell & K_{s2}\cdot\ell & -2(K_{s1}+K_{s2}) & K_{s1}\cdot\ell & K_{s2}\cdot\ell \\ K_{s1}\cdot\ell & K_{s1}\frac{\ell^2}{2}+2K_{b1}+2K_1\cdot\ell & K_3\cdot\ell & -K_{s1}\cdot\ell & K_{s1}\frac{\ell^2}{2}-2K_{b1} & 0 \\ K_{s2}\cdot\ell & K_3\cdot\ell & K_{s2}\frac{\ell^2}{2}+2K_{b2}+2K_2\cdot\ell & -K_{s2}\cdot\ell & 0 & K_{s2}\frac{\ell^2}{2}-2K_{b2} \\ -2(K_{s1}+K_{s2}) & -K_{s1}\cdot\ell & -K_{s2}\cdot\ell & 2(K_{s1}+K_{s2}) & -K_{s1}\cdot\ell & -K_{s2}\cdot\ell \\ K_{s1}\cdot\ell & K_{s1}\frac{\ell^2}{2}-2K_{b1} & 0 & -K_{s1}\cdot\ell & K_{s1}\frac{\ell^2}{2}+2K_{b1}+2K_1\cdot\ell & K_3\cdot\ell \\ K_{s2}\cdot\ell & 0 & K_{s2}\frac{\ell^2}{2}-2K_{b2} & -K_{s2}\cdot\ell & K_3\cdot\ell & K_{s2}\frac{\ell^2}{2}+2K_{b2}+2K_2\cdot\ell \end{bmatrix} \tag{A.2}$$

where

$$\begin{cases} K_1 = \frac{EI_b}{\lambda\ell_b}\left(\frac{12\bar{\alpha}^2}{\ell_b^2}-\frac{12\bar{\alpha}}{\ell_b}+3+\lambda\right); \quad K_{s1}=G\kappa A_1; \quad K_{s2}=G\kappa A_2 \\ K_2 = \frac{EI_b}{\lambda\ell_b}\left(\frac{12\bar{\beta}^2}{\ell_b^2}-\frac{12\bar{\beta}}{\ell_b}+3+\lambda\right); \quad K_{b1}=EI_1; \quad K_{b2}=EI_2 \\ K_3 = \frac{EI_b}{\lambda\ell_b}\left(\frac{24\bar{\alpha}\bar{\beta}}{\ell_b^2}-\frac{12\bar{\alpha}+12\bar{\beta}}{\ell_b}+6-2\lambda\right) \\ \lambda = 1+12r; \quad r=\frac{EI_b}{G\kappa A_b\ell_b^2}; \quad \bar{\alpha}=-\frac{B_1}{2}; \quad \bar{\beta}=\frac{B_2}{2} \end{cases} \tag{A.3}$$

The FE damping matrix C_e, which includes the classical, shear, and bending damping, is given by

$$C_e = \frac{\ell}{2}\begin{bmatrix} \frac{2}{3}c+\frac{2c_{s1}\kappa A_1}{\ell^2}+\frac{2c_{s2}\kappa A_2}{\ell^2} & \frac{c_{s1}\kappa A_1}{\ell} & \frac{c_{s2}\kappa A_2}{\ell} & \frac{1}{3}c-\frac{2c_{s1}\kappa A_1}{\ell^2}-\frac{2c_{s2}\kappa A_2}{\ell^2} & \frac{c_{s1}\kappa A_1}{\ell} & \frac{c_{s2}\kappa A_2}{\ell} \\ \frac{c_{s1}\kappa A_1}{\ell} & \frac{c_{s1}\kappa A_1}{\ell}+2c_{b1}I_1+\frac{2C_1}{\ell} & \frac{C_3}{\ell} & -\frac{c_{s1}\kappa A_1}{\ell} & \frac{c_{s1}\kappa A_1}{\ell}-2c_{b1}I_1 & 0 \\ \frac{c_{s2}A_2}{\ell} & \frac{C_3}{\ell} & \frac{c_{s2}\kappa A_2}{\ell}+2c_{b2}I_2+\frac{2C_2}{\ell} & -\frac{c_{s2}\kappa A_2}{\ell} & 0 & \frac{c_{s2}\kappa A_2}{\ell}-2c_{b2}I_2 \\ \frac{1}{3}c-\frac{2c_{s1}\kappa A_1}{\ell^2}-\frac{2c_{s2}\kappa A_2}{\ell^2} & -\frac{c_{s1}\kappa A_1}{\ell} & -\frac{c_{s2}\kappa A_2}{\ell} & \frac{2}{3}c+\frac{2c_{s1}\kappa A_1}{\ell^2}+\frac{2c_{s2}\kappa A_2}{\ell^2} & -\frac{c_{s1}A_1}{\ell} & -\frac{c_{s2}\kappa A_2}{\ell} \\ \frac{c_{s1}\kappa A_1}{\ell} & \frac{c_{s1}\kappa A_1}{\ell}-2c_{b1}I_1 & 0 & -\frac{c_{s1}\kappa A_1}{\ell} & \frac{c_{s1}\kappa A_1}{\ell}+2c_{b1}I_1+\frac{2C_1}{\ell} & \frac{C_3}{\ell} \\ \frac{c_{s2}\kappa A_2}{\ell} & 0 & \frac{c_{s2}\kappa A_2}{\ell}-2c_{b2}I_2 & -\frac{c_{s2}\kappa A_2}{\ell} & \frac{C_3}{\ell} & \frac{c_{s2}\kappa A_2}{\ell}+2c_{b2}I_2+\frac{2C_2}{\ell} \end{bmatrix} \tag{A.4}$$

where

$$\begin{cases} C_1 = c_{b3}I_b\left(\frac{4}{3\lambda^2\ell_b}+m_1^2\ell_b-\frac{2m_1}{\lambda}\right)+\ell_b c_{s3}\kappa A_b m_3^2 \\ C_2 = c_{b3}I_b\left(\frac{4}{3\lambda^2\ell_b}+m_2^2\ell_b+\frac{2m_2}{\lambda}\right)+\ell_b c_{s3}\kappa A_b m_4^2 \\ C_3 = 2c_{b3}I_b\left(2m_1m_2\ell_b-\frac{8}{3\lambda^2\ell_b}+\frac{2m_1-2m_2}{\lambda}\right)+2c_{s3}\kappa A_b(m_3m_4\ell_b) \\ m_1 = \frac{3+\lambda}{\lambda\ell_b}-\frac{3B_1}{\lambda\ell_b^2}; \quad m_2 = \frac{3-\lambda}{\lambda\ell_b}-\frac{3B_2}{\lambda\ell_b^2} \\ m_3 = \frac{\lambda-1}{2\lambda}\left(1-\frac{B_1}{\ell_b}\right); \quad m_4 = \frac{\lambda-1}{2\lambda}\left(1-\frac{B_2}{\ell_b}\right) \end{cases} \tag{A.5}$$

The generalized forces vector Q_e is expressed as follows

$$Q_e = \frac{f(t)\ell}{2}[\,1 \quad 0 \quad 0 \quad 1 \quad 0 \quad 0\,]^T \tag{A.6}$$

The functions of displacement and rotation in the connecting beams of coupled shear walls are, respectively

$$v(y) = \left[(m_3+1)y+\frac{1}{2}m_1y^2-\frac{y^3}{3\ell_b^2}-\frac{B_1}{2}\right]\theta+\left[m_4y+\frac{1}{2}m_2y^2+\frac{y^3}{3\ell_b^2}\right]\psi \tag{A.7}$$

$$\varphi(y) = \left[m_1y-\frac{y^2}{\ell_b^2}+1\right]\theta+\left[m_2y+\frac{y^2}{\ell_b^2}\right]\psi \tag{A.8}$$

Appendix B

Concerning the continuum-based model (GSB), the contribution of the continuum core to the FE mass matrix is

$$M_{core} = \frac{\ell}{2}\begin{bmatrix} \frac{2\gamma_u}{3} & 0 & 0 & \frac{\gamma_u}{3} & 0 & 0 \\ 0 & \frac{B_1^2\gamma_\rho}{6\ell_b^2} & \frac{B_1B_2\gamma_\rho}{6\ell_b^2} & 0 & \frac{B_1^2\gamma_\rho}{12\ell_b^2} & \frac{B_1B_2\gamma_\rho}{12\ell_b^2} \\ 0 & \frac{B_1B_2\gamma_\rho}{6\ell_b^2} & \frac{B_2^2\gamma_\rho}{6\ell_b^2} & 0 & \frac{B_1B_2\gamma_\rho}{12\ell_b^2} & \frac{B_2^2\gamma_\rho}{12\ell_b^2} \\ \frac{\gamma_u}{3} & 0 & 0 & \frac{2\gamma_u}{3} & 0 & 0 \\ 0 & \frac{B_1^2\gamma_\rho}{12\ell_b^2} & \frac{B_1B_2\gamma_\rho}{12\ell_b^2} & 0 & \frac{B_1^2\gamma_\rho}{6\ell_b^2} & \frac{B_1B_2\gamma_\rho}{6\ell_b^2} \\ 0 & \frac{B_1B_2\gamma_\rho}{12\ell_b^2} & \frac{B_2^2\gamma_\rho}{12\ell_b^2} & 0 & \frac{B_1B_2\gamma_\rho}{6\ell_b^2} & \frac{B_2^2\gamma_\rho}{6\ell_b^2} \end{bmatrix} \tag{B.1}$$

where: $\gamma_u = \rho_d\cdot(t\ell_b)$; $\gamma_\rho = \rho_d\cdot\left(\frac{t\ell_b^3}{12}\right)$.

Also, the FE stiffness matrix associated to the continuum core of the GSB reads

$$K_{core} = G_{eq}(t\kappa\ell_b)\begin{bmatrix} \frac{1}{\ell} & -\frac{B_1}{4\ell_b} & -\frac{B_2}{4\ell_b} & -\frac{1}{\ell} & -\frac{B_1}{4\ell_b} & -\frac{B_2}{4\ell_b} \\ -\frac{B_1}{4\ell_b} & \frac{B_1^2\ell}{16\ell_b^2} & \frac{B_1B_2\ell}{16\ell_b^2} & \frac{B_1}{4\ell_b} & \frac{B_1^2\ell}{16\ell_b^2} & \frac{B_1B_2\ell}{16\ell_b^2} \\ -\frac{B_2}{4\ell_b} & \frac{B_1B_2\ell}{16\ell_b^2} & \frac{B_2^2\ell}{16\ell_b^2} & \frac{B_2}{4\ell_b} & \frac{B_1B_2\ell}{16\ell_b^2} & \frac{B_2^2\ell}{16\ell_b^2} \\ -\frac{1}{\ell} & \frac{B_1}{4\ell_b} & \frac{B_2}{4\ell_b} & \frac{1}{\ell} & \frac{B_1}{4\ell_b} & \frac{B_2}{4\ell_b} \\ -\frac{B_1}{4\ell_b} & \frac{B_1^2\ell}{16\ell_b^2} & \frac{B_1B_2\ell}{16\ell_b^2} & \frac{B_1}{4\ell_b} & \frac{B_1^2\ell}{16\ell_b^2} & \frac{B_1B_2\ell}{16\ell_b^2} \\ -\frac{B_2}{4\ell_b} & \frac{B_1B_2\ell}{16\ell_b^2} & \frac{B_2^2\ell}{16\ell_b^2} & \frac{B_2}{4\ell_b} & \frac{B_1B_2\ell}{16\ell_b^2} & \frac{B_2^2\ell}{16\ell_b^2} \end{bmatrix} \tag{B.2}$$

The FE damping matrix contributed to the continuum core in the GSB is expressed as

$$C_{core} = c_{eq}(t\kappa\ell_b)\frac{\ell}{2}\begin{bmatrix} \frac{2}{\ell^2} & -\frac{B_1}{2\ell\ell_b} & -\frac{B_2}{2\ell\ell_b} & -\frac{2}{\ell^2} & -\frac{B_1}{2\ell\ell_b} & -\frac{B_2}{2\ell\ell_b} \\ -\frac{B_1}{2\ell\ell_b} & \frac{B_1^2}{8\ell_b^2} & \frac{B_1B_2}{8\ell_b^2} & \frac{B_1}{2\ell\ell_b} & \frac{B_1^2}{8\ell_b^2} & \frac{B_1B_2}{8\ell_b^2} \\ -\frac{B_2}{2\ell\ell_b} & \frac{B_1B_2}{8\ell_b^2} & \frac{B_2^2}{8\ell_b^2} & \frac{B_2}{2\ell\ell_b} & \frac{B_1B_2}{8\ell_b^2} & \frac{B_2^2}{8\ell_b^2} \\ -\frac{2}{\ell^2} & \frac{B_1}{2\ell\ell_b} & \frac{B_2}{2\ell\ell_b} & \frac{2}{\ell^2} & \frac{B_1}{2\ell\ell_b} & \frac{B_2}{2\ell\ell_b} \\ -\frac{B_1}{2\ell\ell_b} & \frac{B_1^2}{8\ell_b^2} & \frac{B_1B_2}{8\ell_b^2} & \frac{B_1}{2\ell\ell_b} & \frac{B_1^2}{8\ell_b^2} & \frac{B_1B_2}{8\ell_b^2} \\ -\frac{B_2}{2\ell\ell_b} & \frac{B_1B_2}{8\ell_b^2} & \frac{B_2^2}{8\ell_b^2} & \frac{B_2}{2\ell\ell_b} & \frac{B_1B_2}{8\ell_b^2} & \frac{B_2^2}{8\ell_b^2} \end{bmatrix} \tag{B.3}$$

Appendix C

The base moment time-history $M_b(t)$ reads:

$$M_b(t) = \sum_{j=1}^{n}\left\{\frac{(K_b\lambda_j^2 - k_\vartheta)}{\lambda_j}\left[\eta_j\sinh(\lambda_j) - \frac{\gamma_j}{\lambda_j}\cosh(\lambda_j)\right] + \frac{k_\vartheta + K_b\gamma_j^2}{\gamma_j}[\cos(\gamma_j) + \eta_j\sin(\gamma_j)] - k_\vartheta\frac{\lambda_j^2+\gamma_j^2}{\gamma_j\lambda_j^2}\right\}\Gamma_j D_j(t) \tag{C.1}$$

and the base shear time-history $V_b(t)$ can be expressed by

$$V_b(t) = \sum_{j=1}^{n}\left\{\left(k_\vartheta + K_b\gamma_j^2\right)[\eta_j\cos(\gamma_j) - \sin(\gamma_j)] + \left(k_\vartheta - K_b\lambda_j^2\right) \times\left[\frac{\gamma_j}{\lambda_j}\sinh(\lambda_j) - \eta_j\cosh(\lambda_j)\right] - K_b\left(\gamma_j^2+\lambda_j^2\right)\eta_j\right\}\Gamma_j D_j(t) \tag{C.2}$$

References

[1] Kwan AKH, Cheung YK. Analysis of coupled shear/core walls using a beam-type finite element. Eng Struct 1994;16(2):111–8.
[2] Zalka KA. A simplified method for calculation of the natural frequencies of wall-frame buildings. Eng Struct 2001;23(12):1544–55.
[3] Aksogan O, Arslan HM, Choo BS. Forced vibration analysis of stiffened coupled shear walls using continuous connection method. Eng Struct 2003;25 (4):499–506.
[4] Potzta G, Kollar LP. Analysis of building structures by replacement sandwich beams. Int J Solids Struct 2003;40(3):535–53.
[5] Dym CL, Williams HE. Estimating fundamental frequencies of tall buildings. J Struct Eng 2007;135(9):1479–83.
[6] Meftah SA, Tounsi A, El Abbas AB. A simplified approach for seismic calculation of a tall building braced by shear walls and thin-walled open section structures. Eng Struct 2007;29(10):2576–85.
[7] Adhikari S. Damping models for structural vibration. Ph.D. Thesis. Cambridge University; 2000.
[8] Adihikari S, Woodhous J. Identification of damping: Part 1, viscous damping. J Sound Vib 2001;243(1):43–61.
[9] Muravskii GB. On frequency independent damping. J Sound Vib 2004;274(3–5):653–68.
[10] Zarubinskaya MA, Van Horssen WT. On an improved elastic dissipation model for a cantilevered beam. Quart Appl Math 2005;63(4):681–90.
[11] De Silva CW. Vibration damping, control, and design. CRC Press, Taylor and Francis Group; 2007.
[12] Boudaoud H, Daya EM, Belouettar S, Duigou L, Potier-Ferry M. Damping analysis of beams submitted to passive and active control. Eng Struct 2009;31 (2):322–31.
[13] Kocatürk T, ¸Simşek M. Dynamic analysis of eccentrically prestressed viscoelastic Timoshenko beams under a moving harmonic force. Comput Struct 2006;84(31–32):2113–27.
[14] Kayacık O, Bruch JC, Sloss JM, Adali S, Sadek IS. Integral equation approach for piezo patch vibration control of beams with various types of damping. Comput Struct 2008;86(3–5):357–66.
[15] Tsai TC, Tsau JH, Chen CS. Vibration analysis of a beam with partially distributed internal viscous damping. Int J Mech Sci 2009;51(11–12):907–14.
[16] Chen WR. Bending vibration of axially loaded Timoshenko beams with locally distributed Kelvin–Voigt damping. J Sound Vib 2011;330(13):3040–56.
[17] Capsoni A, Vigano GM, Bani-Hani K. On damping effects in Timoshenko beams. Int J Mech Sci 2013;73:27–39.
[18] Faridani HM, Capsoni A. An innovative approach to model dissipation mechanism in coupled shear walls. In: Proceedings of the 9th international conference on structural dynamics, EURODYN 2014, Porto, Portugal, 30 June–2 July. p. 1679–88.
[19] Lavan O. On the efficiency of viscous dampers in reducing various seismic responses of wall structures. Earthquake Eng Struct Dyn 2012;41 (12):1673–92.
[20] Christopoulos C, Montgomery M. Viscoelastic coupling dampers (VCDs) for enhanced wind and seismic performance of high-rise buildings. Earthquake Eng Struct Dyn 2013;42:2217–33.
[21] Miranda E, Taghavi SH. Approximate floor acceleration demands in multistory buildings. I: Formulation. J Struct Eng 2005;131(2):203–11.
[22] Hunt BR, Lipsman RL, Rosenberg J. A guide to Matlab: for beginners and experienced users. Cambridge University Press; 2006.
[23] McMahon D, Topa DM. A beginner's guide to mathematica. Chapman & Hall/CRC; 2006.
[24] Clough RW, Penzien J. Dynamics of structures Inc, Berkeley, computers and structures, 3rd ed. USA, Berkeley; 2003.
[25] Takabatake H. Two-dimensional rod theory for approximate analysis of building structures. Earthquakes Struct 2010;1(1):1–19.
[26] Capuani D, Merli M, Savoia M. An equivalent continuum approach for coupled shear walls. Eng Struct 1994;16(1):63–73.
[27] Capuani D, Merli M, Savoia M. Dynamic analysis of coupled shear wall-frame systems. J Sound Vib 1996;192(4):867–83.
[28] Smith BS, Coull A. Tall building structures: analysis and design. New York: John Wily & Sons; 1991.
[29] Tounsi A, Houari MSA, Benyoucef S, Bedia EAA. A refined trigonometric shear deformation theory for thermoelastic bending of functionally graded sandwich plates. Aerosp Sci Technol 2013;24:209–20.
[30] Bouderba B, Houari MSA, Tounsi A. Thermomechanical bending response of FGM thick plates resting on Winkler–Pasternak elastic foundations. Steel Compos Struct 2013;4(1):85–104.
[31] Zidi M, Tounsi A, Houari MSA, Bedia EAA, Anwar Bég O. Bending analysis of FGM plates under hygro-thermo-mechanical loading using a four variable refined plate theory. Aerosp Sci Technol 2014;34:24–34.
[32] Belabed Z, Houari MSA, Tounsi A, Mahmoud SR, Anwar Bég O. An efficient and simple higher order shear and normal deformation theory for functionally graded material (FGM) plates. Composites: Part B 2014;60:274–83.
[33] Bousahla AA, Houari MSA, Tounsi A, Bedia EAA. A novel higher order shear and normal deformation theory based on neutral surface position for bending analysis of advanced composite plates. Int J Comput Meth 2014;11(6):, 1350082.
[34] Meziane MAA, Abdelaziz HH, Tounsi A. An efficient and simple refined theory for buckling and free vibration of exponentially graded sandwich plates under various boundary conditions. J Sandwich Struct Mater 2014;16(3):293–318.
[35] Neves AMA, Ferreira AJM, Carrera E, Cinefra M, Roque CMC, Jorge RMN, Soares MCM. A new quasi-3D hyperbolic shear deformation theory for the static and free vibration analysis of functionally graded plates. ASCE J Eng Mech 2014;140:374–83.
[36] Draiche K, Tounsi A, Khalfi Y. A trigonometric four variable plate theory for free vibration of rectangular composite plates with patch mass. Steel Compos Struct 2014;17(1):69–81.
[37] Yahia SA, Atmane HA, Houari MSA, Tounsi A. Wave propagation in functionally graded plates with porosities using various higher-order shear deformation plate theories. Struct Eng Mech 2015;53(6):1143–65.
[38] Larbi LO, Kaci A, Houari MSA, Tounsi A. An efficient shear deformation beam theory based on neutral surface position for bending and free vibration of functionally graded beams. Mech Des Struct Mach 2013;41:421–33.
[39] Bourada M, Kaci A, Houari MSA, Tounsi A. A new simple shear and normal deformations theory for functionally graded beams. Steel Compos Struct 2015;18(2):409–23.
[40] Al-Basyouni KS, Tounsi A, Mahmoud SR. Size dependent bending and vibration analysis of functionally graded micro beams based on modified couple stress theory and neutral surface position. Compos Struct 2015;125:621–30.
[41] Capsoni A, Faridani HM. Novel continuum models for coupled shear wall analysis. Struct Des Tall Special Build 2015. http://dx.doi.org/10.1002/tal.1267.
[42] Chen Y, McFarland DM, Wang Z, Spencer BF, Bergman LA. Analysis of tall buildings with damped outriggers. J Struct Eng 2010;136(11):1435–43.
[43] Takewaki I. Optimal damper placement for minimum transfer functions. Earthquake Eng Struct Dyn 1997;26:1113–24.
[44] Smith R, Willford MR. The damped outrigger concept for tall buildings. Struct Des Tall Special Build 2007;16:501–17.
[45] Satake N, Suda KI, Arakawa T, Sasaki A, Tamura Y. Damping evaluation using full-scale data of buildings in Japan. J Struct Eng 2003;129:470–7.
[46] Jeary AP. Damping in tall buildings – a mechanism and a predictor. Earthquake Eng Struct Dyn 1986;14(5):733–50.
[47] Li QS, Liu DK, Fang JQ, Jeary AP, Wong CK. Damping in buildings: its neural network model and AR model. Eng Struct 2000;22(9):1216–23.
[48] Jeary AP. The description and measurement of nonlinear damping in structures. J Wind Eng Ind Aerodyn 1996;59:103–14.
[49] Jeary AP. Damping in structures. J Wind Eng Ind Aerodyn 1997;72: 345–55.

[50] Lagomarsino S. Forecast models for damping and vibration periods of buildings. J Wind Eng Ind Aerodyn 1993;48(2–3):221–39.
[51] Tamura Y. Amplitude dependency of damping in buildings and critical tip drift ratio. Int J High-Rise Build 2012;1(1):1–13.
[52] Tamura Y, Suda K, Sasaki A. Damping in buildings for wind resistant design. In: Proceedings of the international symposium on wind and structures for the 21st century, Korea, Cheju, 26–28 January; 2000. p. 115–30.
[53] Spence SMJ, Kareem A. Tall buildings and damping: a concept-based data-driven model. J Struct Eng 2014;140(5):1–15.
[54] Aquino RER, Tamura Y. Framework for structural damping predictor models based on stick-slip mechanism for use in wind-resistant design of buildings. J Wind Eng Ind Aerodyn 2013;117:25–37.